Assessing Mild Cognitive Impairment Progression using a Spherical Brain Mapping of Magnetic Resonance Imaging

Francisco Jesus Martinez-Murcia[1]*, Juan Manuel Górriz[1,2], Javier Ramírez[1], Fermín Segovia[1], Diego Salas-Gonzalez[1], Diego Castillo-Barnes[1], Andrés Ortiz[3]

[1]Dept. of Signal Theory, Networking and Communications
18071 University of Granada, Spain

[2]Department of Psychiatry
CB2 0SZ, University of Cambridge, UK

[3]Dpt. of Communications Engineering
29071 University of Málaga, Spain

for the Alzheimer's Disease Neuroimaging Initiative†

January 30, 2018

Abstract

***Background**: The early diagnosis of Alzheimer's Disease (AD), particularly in its prodromal stage, Mild Cognitive Impairment (MCI) remains still a challenge. Many computational tools have been developed to successfully explore and predict the disease progression. In this context, the Spherical Brain Mapping (SBM) proved its ability in detecting differences between AD and aged subjects without symptoms of dementia. Being a very visual tool, its application in predicting MCI conversion to AD could be of great help to understand neurodegeneration and the disease progression. **Objective**: In this work we aim at: predicting the conversion of MCI affected subjects to AD more than 6 months in advance of their conversion session and understanding the progression of the disease by predicting neuropsychological test outcomes from MRI data. **Methods**: In order to do so, SBM is applied to a series of MRI scans from the Alzheimer's Disease Neuroimaging Initiative (ADNI). The resulting spherical brain maps show statistical and morphological information of the brain in a bidimensional plane, performing at the same time a significant feature reduction, that provides a feature vector used in classification analysis. **Results**: The study achieves up to 92.3% accuracy in the AD vs normal controls (CTL) detection, and up to a 77.6% in detection a of MCI conversions when trained with AD and CTL subjects. The prediction of neuropsychological test outcomes achieved R^2 rates up to more than 0.5. Significant regions according to t-test and correlation analysis match reported brain areas in the literature. **Conclusion**: The results prove that Spherical Brain Mapping offers good ability to predict conversion patterns and cognitive state, at the same time that provides an additional aid for visualizing a two-dimensional abstraction map of the brain.*

Keywords: Alzheimer Disease, Cognitive Dysfunction, Magnetic Resonance Imaging, Classification, Regression Analysis, Disease Progression

*Corresponding author: Francisco Jesus Martinez-Murcia. C/ Periodista Rafael Gomez 2, D1-5. 18071 Granada (Spain). Tlfn. +34 958 241717. Email: fjesusmartinez@ugr.es

†Data used in preparation of this article were obtained from the Alzheimer's Disease Neuroimaging Initiative (ADNI) database (adni.loni.usc.edu). As such, the investigators within the ADNI contributed to the design and implementation of ADNI and/or provided data but did not participate in analysis or writing of this report. A complete listing of ADNI investigators can be found at: http://adni.loni.usc.edu/wp-content/uploads/how_to_apply/ADNI_Acknowledgement_List.pdf

I. Introduction

Alzheimer's Disease (AD) is the most common neurodegenerative disorder in the world, with more than 46 million affected, a number that is expected to grow up to 131.5 million by 2050 [2]. Many computational tools have been developed to aid in the diagnosis of AD, however, its early diagnosis remains a challenge, especially in its prodromal stage known as Mild Cognitive Impairment (MCI). The early and more accurate diagnosis of possible AD would reduce the mistreatment of MCI and an earlier treatment of the disease when its symptoms are still subtle. This might positively impact the progression of AD, delaying the apparition of a more severe symptomatology and improving the life expectancy and quality of life of the patients and their families.

Currently, cognitive testing is often used to guide in the diagnosis procedure. Clinical tests such as Mini Mental State Exam (MMSE) [33] or the Alzheimer's Disease Assessment Scale-cognitive subscale (ADAS-cog, in 11 and 13-question variants) [3] are often used to assess cognitive decline in patients in risk of suffering AD. However, recent studies [15, 34] show that non-specific neuropsychological scores such as MMSE could be a possible source of false positives in MCI diagnosis.

Neuroimaging, with its ability to perform *in vivo* exploration of brain structure and function, could be a key source of information to enhance MCI diagnosis. Many works have explored the possibility of multivariate analyses of structural and functional imaging using techniques such as Principal Component Analysis [14, 28], Support Vector Machines [24, 16, 10], texture analysis [35, 22, 19] or volume and shape analysis [5, 23, 27, 26, 6, 8]. These works used semi-automatic methodology to segment and extract features from images that leaded to higher discriminative Computer Aided Diagnosis (CAD) systems [18], offering performances up to 80% in the diagnosis of MCI.

Obtaining reliable and objective information from neuroimaging data could effectively increase the accuracy of MCI diagnosis. For its part, predicting neuropsychological tests outcomes could help to understand the relationship between structural changes in the brain and cognitive state (as measured by cognitive tests). This is key to validate diagnostics and establish a connection between neuroimaging and clinical tests. However, only a few works such as [9] attempt to predict cognitive test outcomes.

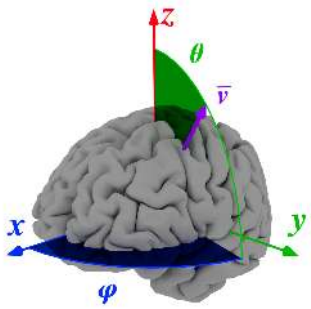

Figure 1: Definition of the mapping vector $\mathbf{v}_{\theta,\varphi}$ and the spherical coordinates.

In this work we will evaluate the usefulness of the Spherical Brain Mapping (SBM) texture measures [20] in two main environments: to predict conversion of MCI subjects and to predict outcomes of different cognitive tests such as MMSE, ADAS-11 and ADAS-13. In the first case, we will use a Support Vector Machine classifier (SVC) to classify the derived SBM maps, as in [24]. For predicting test outcomes, we will test two regression models [25]: Support Vector Machine regression (SVR, Sec. II.3.1) with linear kernel, a robust and generalizable model even in high-dimensional spaces [4], and a Least Absolute Shrinkage and Selection Operator (LASSO, Sec. II.3.2), that estimates sparse coefficients and can therefore be used for feature selection [36]. In addition to this, we will identify and visualize (II.2) the brain areas more related to disease progression using hypothesis testing and correlation analysis. We will test our approaches on MRI data from the Alzheimer's Disease Neuroimaging Initiative (ADNI) [33], whose results can be found at Section III and discussed at Section IV. Finally, we draw some conclusions about this work at section V.

II. Methods

II.1. Spherical Brain Mapping

The Spherical Brain Mapping (SBM) is a framework proposed at [20], whose main feature is to project three dimensional structural brain images to bidimensional maps representing the spatial distribution of a certain texture measure. To do so, it constructs a mapping vector $\mathbf{v}_{\theta,\varphi}$ in the spherical coordinates whose direction is represented by θ and φ (elevation and azimuth, Figure 1) from a given origin of coordinates. While in [20] the geometric centre of the images was used, in this work we set the origin at the Anterior

Commissure, given its favourable anatomical position. All the intensities of the voxels crossed by $\mathbf{v}_{\theta,\varphi}$ define the set of selected intensities $V_{\theta,\varphi}$. 181×361 sets at each of the elevation and azimuth values $0 < \theta < 180$ and $0 < \varphi < 360$ are built at an angular resolution of 1^o. Finally, five statistical and one morphological measures are derived from these intensity sets: average, entropy, kurtosis, skewness and variance (see some examples at Figure 2).

The average of $V_{\theta,\varphi}$ is defined as:

$$v_{average} = \frac{1}{N}\sum_{i=1}^{N} V^i_{\theta,\varphi} \tag{1}$$

where $V^i_{\theta,\varphi}$ is the i^{th} element in the sampled set $V_{\theta,\varphi}$, and N is its size. The entropy of $V_{\theta,\varphi}$, is estimated as:

$$v_{entropy} = \sum_{i=1}^{N} V^i_{\theta,\varphi}\log(V^i_{\theta,\varphi}) \tag{2}$$

The remaining values are computed using the general formula for the r^{th} moment:

$$m_r = \frac{1}{N}\sum_{i=1}^{N}(V^i_{\theta,\varphi} - v_{average})^r \tag{3}$$

from which we derive the corrected variance, skewness and uncorrected kurtosis:

$$v_{variance} = \frac{N}{N-1}m_2 \tag{4}$$

$$v_{skewness} = \frac{m_3}{m_2^{3/2}} \tag{5}$$

$$v_{kurtosis} = \frac{m_3}{m_2^2} \tag{6}$$

And finally, the only morphological measure: the thickness of the tissues crossed by $\mathbf{v}_{\theta,\varphi}$. In this approach, the value is obtained from the indexes (positions) where the intensities are higher than a threshold:

$$V_{idx} = \arg\{V_{\theta,\varphi} > I_{th}\} \tag{7}$$

where I_{th} is the intensity threshold, typically 0. The thickness is defined as:

$$v_{thickness} = \max\{V_{idx}\} - \min\{V_{idx}\} \tag{8}$$

Once we have computed the different measures at each coordinate pair, we can build the SBM maps by putting each value at its corresponding pair. This way, we obtain maps such as the ones presented in Figures 2 and 3. The python package used has been uploaded at `http://github.com/SiPBA/mapBrain`.

II.2. Visualization

II.2.1 Hypothesis Testing

A widespread technique for assessing where class differences are located is hypothesis testing. In this context, we assume a null hypothesis of H_0, that is, the hypothesis that there is no difference between two populations. On the other hand, we formulate the alternative hypothesis H_1: the assumption that there are some differences. Then, a statistical test is applied, from which a certain p-value -the probability of rejecting H_0 by chance- can be derived.

The t-test is a hypothesis testing statistic extensively used in the neuroimaging community, since it is the basis for the SPM and VBM analyses [13]. In this work, we will apply an independent two-sample t-test [11] to each pixel of the resulting SBM measures, in order to display maps where the more discriminant areas are highlighted.

The t-test used in this work quantifies the differences between two classes assuming normal distribution and independent variances, which most of the SBM measures at different (θ, φ) comply with. Let X_i^f a vector containing the f-th feature of all elements in class i. The t-score of the f-th feature can be computed as:

$$t_f = \frac{\bar{X}_1^f - \bar{X}_2^f}{\sqrt{\frac{\sigma^2_{X_2^f} + \sigma^2_{X_1^f}}{n}}} \tag{9}$$

where $\sigma^2_{X_i^f}$ is the variance and $\bar{X}_i^f$ is the average of the f-the feature within class i.

II.2.2 Pearson's Correlation Coefficient

Correlation maps based on the Pearson's Correlation Coefficient (PCC, also known as Pearson's r) have been generated in order to visually assess which regions are more correlated with test outcomes (MMSE, ADAS-11 and ADAS-13). This is done for each measure value $v_{\theta,\varphi}$ in each direction.:

$$r_{12} = \frac{\sum_i (v^i_{\theta,\varphi} - \bar{v}_{\theta,\varphi})(\mathbf{y}_i - \bar{\mathbf{y}})}{\sqrt{\sum_i (v^i_{\theta,\varphi} - \bar{v}_{\theta,\varphi})^2 (\mathbf{y}_i - \bar{\mathbf{y}})^2}} \tag{10}$$

where $\mathbf{y}_i$ is the test score for the i^{th} subject, and $\bar{\mathbf{y}}$ the mean value of all subjects.

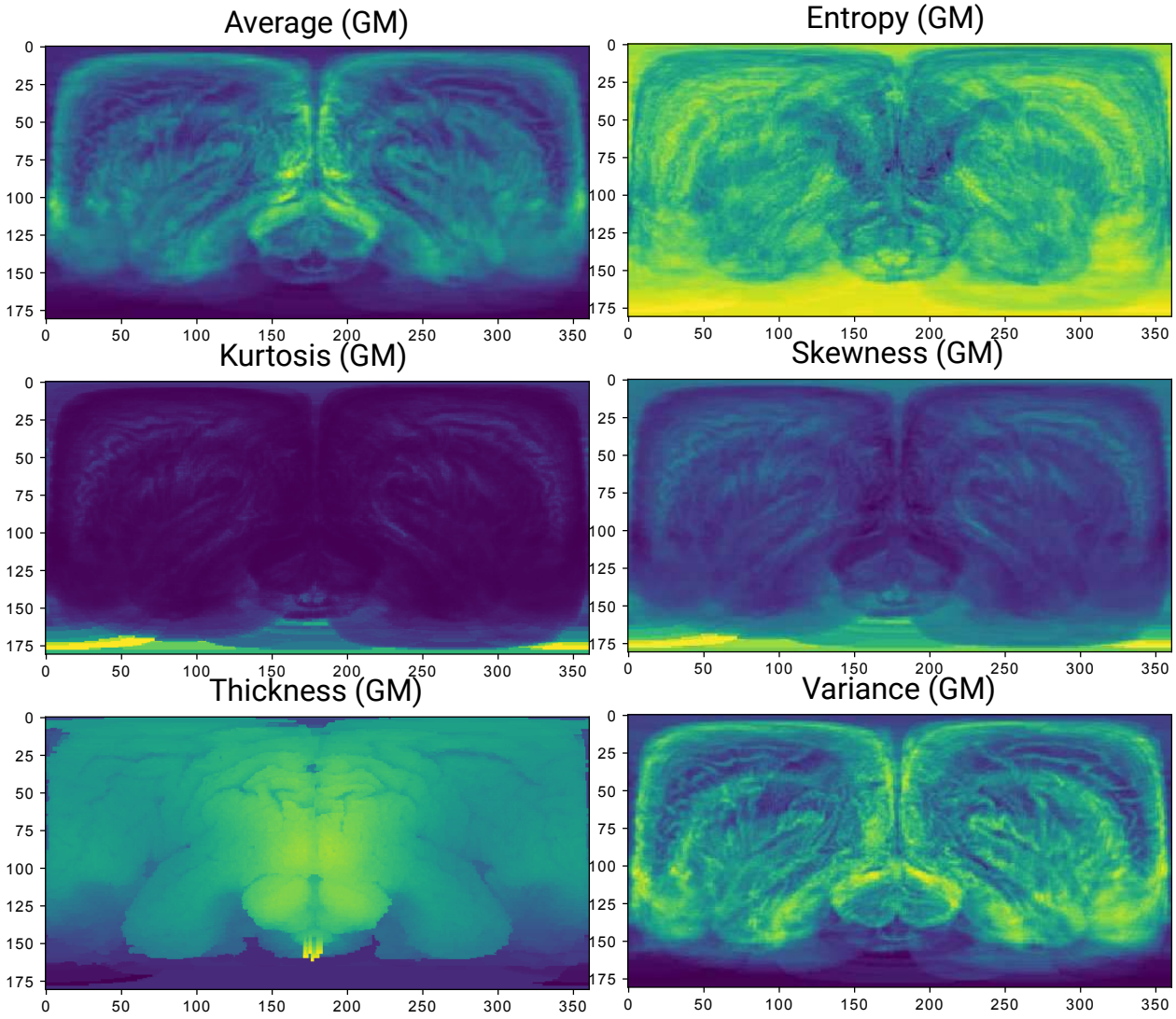

Figure 2: Example of the six SBM maps generated over the GM segmented image of a CTL subject.

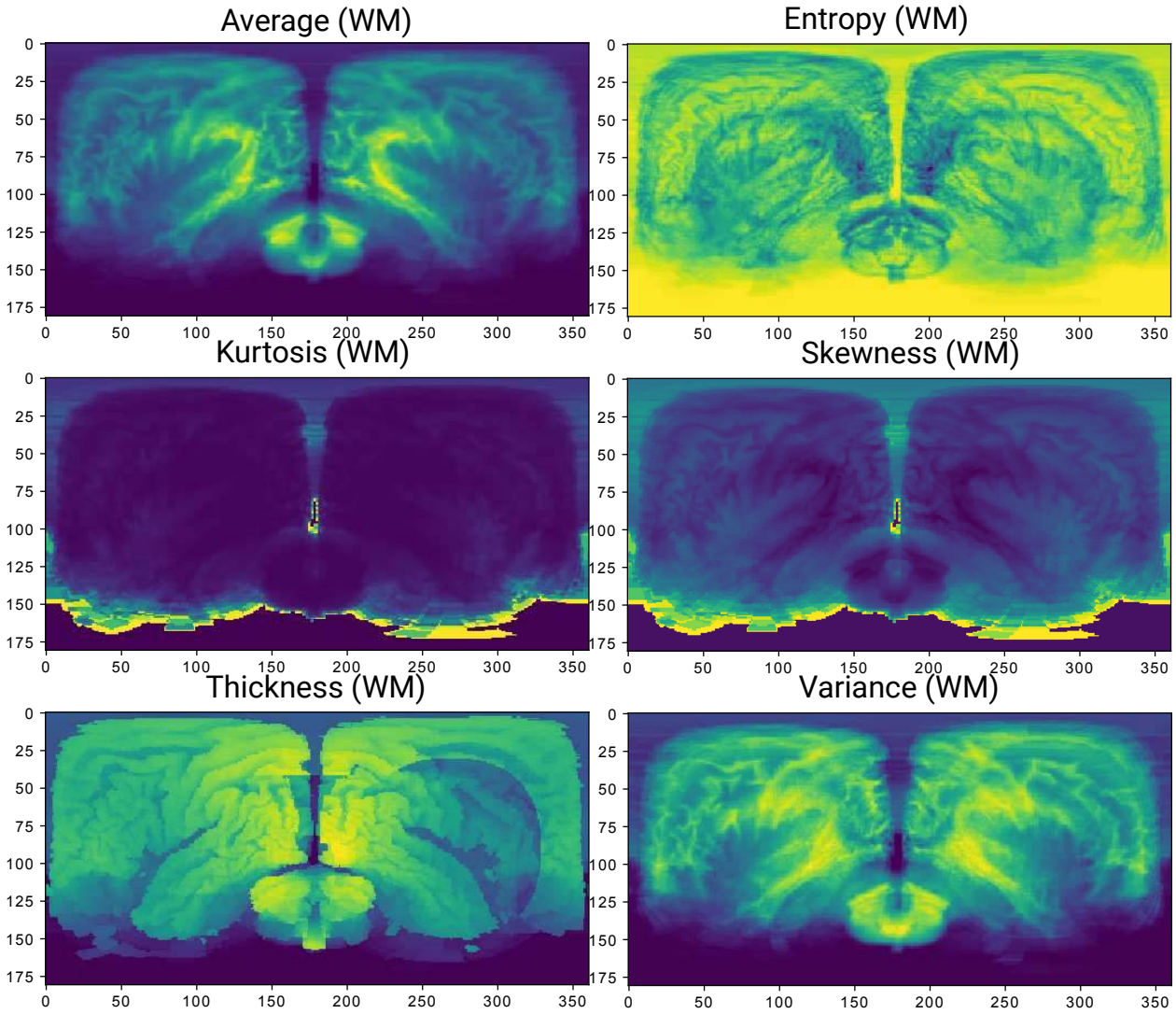

Figure 3: Example of the six SBM maps generated over the WM segmented image of a CTL subject.

II.3. Regression Analysis

II.3.1 Support Vector Regression

Support Vector Regression (SVR) trains Support Vector Machines to predict a continuous variable from previously unseen data [4]. In contrast to the General Lineal Model (GLM) regression, if two features are highly correlated, the computed SVR weights are similar. This is a clear advantage for its use in SBM maps, where the measures are spatially distributed in coordinate pairs, sharing inherent similarities due to neighbourhood. In this work we use the ε-SVR implementation.

For each training vector $\mathbf{x}_i \in \mathbb{R}^p, i = 1, \ldots, n$ (containing each of the n subjects maps), and a vector $\mathbf{y} \in \mathbb{R}^n$ with their corresponding scores ε-SVR solves the following primal problem:

$$\min_{\mathbf{w},b,\zeta,\zeta^*} \frac{1}{2}\mathbf{w}^T\mathbf{w} + C\sum_{i=1}^{n}(\zeta_i + \zeta_i^*) \tag{11}$$

where $\mathbf{w}$ are the SVM coefficients, b is the bias term and the variable $\zeta_i = \max(0, 1 - y_i(w \cdot x_i - b))$. This is subject to the conditions:

$$\mathbf{y}_i - \mathbf{w}^T\mathbf{x}_) - b \leq \varepsilon + \zeta_i, \tag{12}$$

$$\mathbf{w}^T\mathbf{x}_i + b - \mathbf{y}_i \leq \varepsilon + \zeta_i^*, \tag{13}$$

$$\zeta_i, \zeta_i^* \geq 0, i = 1, ..., n \tag{14}$$

where $\varepsilon = 0.1$ is the margin of the hyperplane, and C is a regularization term set to 1. The test scores are therefore predicted using the decision function $f(\mathbf{x}_i) = \mathbf{x}_i\mathbf{w} + b$.

II.3.2 LASSO

Least Absolute Shrinkage and Selection Operator (LASSO) is a regression model that estimates sparse coefficients. This is very useful under the assumption that very few features influence the dependent variable $\mathbf{y}$, and therefore allows performing feature selection and regularization. It is based on a linear model regularized with ℓ_1 prior, defining the following objective function:

$$\min_{\mathbf{w}} \frac{1}{2n}||\mathbf{X}\mathbf{w} - \mathbf{y}||_2^2 + \alpha||\mathbf{w}||_1 \tag{15}$$

where $\mathbf{X} = \mathbf{x}_1, \mathbf{x}_2, \ldots \mathbf{x}_n$ is the training matrix, α is a constant and $||\mathbf{w}||_1$ is the ℓ_1-norm of the parameter vector. The inclusion of the $\alpha||\mathbf{w}||_1$ term solves the minimization of the least-squares penalty. In this work, the LASSO implementation [25] uses coordinate descent to fit the coefficients. Scores are estimated with the decision function $f(\mathbf{x}_i) = \mathbf{x}_i\mathbf{w}^T$.

II.4. Evaluation

II.4.1 ADNI Dataset

Data used in the preparation of this article were obtained from the Alzheimer's Disease Neuroimaging Initiative (ADNI) database (`adni.loni.usc.edu`). The ADNI was launched in 2003 as a public-private partnership, led by Principal Investigator Michael W. Weiner, MD. The primary goal of ADNI has been to test whether serial magnetic resonance imaging (MRI), positron emission tomography (PET), other biological markers, and clinical and neuropsychological assessment can be combined to measure the progression of mild cognitive impairment (MCI) and early Alzheimer's disease (AD).

The database used in this article was obtained with from the ADNI1 initiative, containing subjects that have undergone periodical assessment of cognitive function and MRI acquisition every 6 months, with a total 2182 T1-weighted MRI images (for further information, see `www.adni-info.org`). These images were spatially normalized to the standard SPM template using the SPM8 software [13] Normalize with default parameters (non-rigid, preserve concentrations), and them segmented into Grey Matter (GM) and White Matter (WM) using the VBM8 toolbox.

In the classification experiments we will consider four different cohorts. The first subset correspond to all AD subjects in their baseline acquisition (that is, when the disease is less advanced), and will be regarded as AD from this point. Two more subsets containing the last available visit from CTL and MCI stable will be selected as well, namely the CTL and MCI-S (from MCI stable) subsets. Finally, a MCI subset containing all converters in the last session available prior to their conversion will form the MCI-C (from MCI converter) set.

This choice is not trivial. Since the final aim is to estimate how discriminant are the SBM maps in predicting MCI conversion, we wanted to make the classification task as difficult as possible. Since the MCI-to-AD progression can be viewed as a continuum, the last CTL acquisition will be more difficult to differentiate from the earliest AD, and likewise, the last MCI stable acquisition will be more difficult to differentiate from MCI converters. That way, the MCI-S will be more representative of the whole spectrum commonly classified as MCI but never progress to AD.

For comparison purposes, we will provide the Voxels-As-Features (VAF) [30] performance of this database using the segmented GM and WM maps in

Diag	Gender	N	Age [STD]	MMSE [STD]	ADAS11 [STD]	ADAS13 [STD]
AD	Female	48	75.08 [7.68]	23.11 [2.39]	18.21 [5.88]	28.46 [7.23]
	Male	51	75.37 [7.39]	22.91 [2.43]	19.91 [7.59]	30.02 [9.23]
MCI-C	Female	27	73.04 [8.21]	23.52 [3.09]	13.52 [4.65]	22.72 [5.69]
	Male	43	75.24 [5.51]	24.25 [3.07]	13.19 [4.01]	21.15 [5.52]
MCI-S	Female	15	71.53 [8.41]	25.50 [0.71]	10.19 [4.30]	16.53 [6.27]
	Male	49	75.91 [6.69]	26.33 [1.86]	10.67 [4.40]	17.13 [6.15]
CTL	Female	61	75.94 [4.42]	30.00 [0.00]	5.687 [3.15]	8.350 [4.26]
	Male	61	75.38 [5.72]	29.33 [1.21]	6.645 [2.88]	10.33 [4.22]

Table 1: Demographics of the ADNI dataset.

the AD vs CTL and MCI-C vs MCI-S classification.

II.4.2 Evaluation Parameters

We will test the SBM statistic maps in two different environments: in predicting the conversion of MCI to dementia, and trying to predict neuropsychological test outcomes. The first one is a classification approach, and therefore, we will employ a linear Support Vector Machine classifier (SVC) to estimate how relevant the differences between classes are. The final performance values estimate how discriminant the different measures are when classifying two classes. Accuracy (acc.), Sensitivity (sens.) and Specificity (spec.) and their standard deviation (SD) will be estimated as:

$$acc. = \frac{TP+TN}{N}, \quad sens. = \frac{TP}{TP+FN}, \quad spec. = \frac{TN}{TN+FP} \tag{16}$$

where TP, TN, FP and FN are the number of true positives, true negatives, false positives and false negatives respectively.

The performance estimates are obtained via a stratified 10-fold cross-validation [17]. In brief, this procedure divides the whole dataset in 10 subsets with the same proportion of classes, and iteratively uses 9 of this subsets for training and tests against the remaining one. The procedure is repeated 10 times, from which we obtain the average and standard deviation of the different proposed estimates. Performance estimates of the classification of AD vs CTL groups and MCI converters vs stable will be computed. Since MCI is a rather heterogeneous class, with overlapping converters and non-converters, we additionally will use AD and CTL subjects to train the classifier, and then identify the MCI subjects more similar to AD as converters and those more similar to CTL as stable.

The second environment corresponds to regression analysis. Since SBM maps have never been tested on this environment, we will employ two different strategies: Support Vector Machine regression (SVR, Sec. II.3.1) and a Least Absolute Shrinkage and Selection Operator (LASSO, Sec. II.3.2). To quantify the quality of the prediction of our regressive model, we use the Mean Square Error (MSE) and the coefficient of determination R^2. These performance measures are estimated as the average of all 10 measures computed within a 10-fold cross-validation loop. The MSE measures the mean error of the outcomes of the trained model, and is computed as:

$$MSE = \frac{1}{N}\sum_i (\hat{\mathbf{y}}_i - \mathbf{y}_i)^2 \tag{17}$$

where $\hat{\mathbf{y}}_i$ are the outcomes of the model for the i^{th} subject.

For its part, R^2 measures the proportion of variance in the dependent variable y_i (the outcomes of the cognitive tests) that is explained by the trained model. The best R^2 possible is 1.0, a 0.0 is the score of a constant model that always predicts the expected value of $\mathbf{y}$, and it can be negative (an arbitrarily worse model). It is computed as:

$$R^2 = 1 - \frac{\sum_i (\mathbf{y}_i - \hat{\mathbf{y}}_i)^2}{\sum_i (\mathbf{y}_i - \bar{\mathbf{y}})^2} \tag{18}$$

Furthermore, visual maps for both environments will be provided. For differences between groups, we will use the t-test in each value of the SBM maps. To estimate the correlation of each SBM feature with the neuropsychological test outcomes, we will use the Pearson's r, as defined before.

scenario	tissue	acc. [STD]	sens. [STD]	spec. [STD]
AD vs CTL	GM	0.768[0.011]	0.752[0.016]	0.785[0.016]
	WM	0.642[0.009]	0.668[0.012]	0.617[0.013]
MCI-C vs MCI-S	GM	0.708[0.165]	0.728[0.174]	0.688[0.197]
	WM	0.753[0.122]	0.757[0.157]	0.752[0.139]

Table 2: VAF performance of this dataset.

III. Results

III.1. Anatomical Reference

To better understand the SBM maps, and the location of differences and correlations, we have created two different templates (external -figure 4- and internal -figure 5-, depending on their distance to the crust) that will be used as a reference throughout this section. These templates have been created by projecting each of the regions of the well known Automatic Anatomical Labelling (AAL) atlas [31] by using the SBM-average measure, then smoothing out the projection of each individual region and finally assigning different colours.

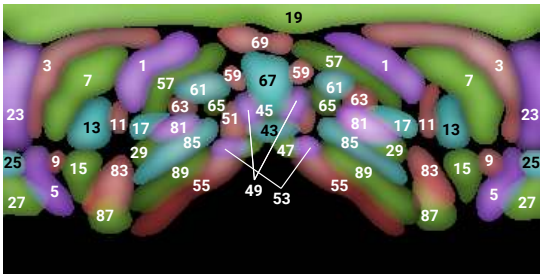

Figure 4: Structures at the cortex projected using SBM, including: 1) Precentral gyrus, 3) frontal superior gyrus, 5) frontal superior orbital gyrus 7) frontal middle gyrus, 9) frontal medial orbital gyrus, 11) frontal inferior operculum, 13) frontal inferior pars triangularis, 15) frontal inferior orbital gyrus, 17) rolandic operculum, 19) superior motor area, 23) frontal superior medial gyrus, 25) frontal medial orbital gyrus, 27) gyrus rectus, 43) calcarine sulcus, 45) cuneus, 47) lingual gyrus, 49) occipital superior gyrus, 51) occipital middle gyrus, 53) occipital inferior gyrus, 55) fusiform gyrus, 57) postcentral gyrus, 61) parietal inferior gyrus, 63) supramarginal gyrus, 65) angular gyrus, 67) precuneus, 69) paracentral lobule, 81) temporal superior gyrus, 83) temporal pole superior part, 85) temporal middle gyrus, 87) temporal pole middle part, 89) temporal inferior gyrus.

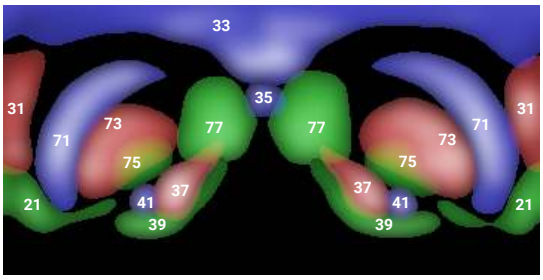

Figure 5: Subcortical structures projected using SBM. Same label is used for both left and right hemisphere as a reference. 21) olfactory bulb, 31) anterior part of the cingulate gyrus, 33) middle part of the cingulate gyrus, 35) posterior part of the cingulate gyrus, 37) hippocampus, 39) parahippocampal gyrus, 41) amygdala, 71) caudate nucleus, 73) putamen, 75) globus pallidus, 77) thalamus.

III.2. Visualization

In this section we focus on the two aforementioned visualization techniques: the hypothesis testing (to assess differences between the AD, MCI-C, MCI-S and CTL groups) and maps that display the correlation between SBM measures and neuropsychological tests.

III.2.1 Differences Between Groups

In Figure 6 we show the significant regions (uncorrected t-test, $p<0.001$) of each SBM measure computed over the GM tissue. In these maps we can see shapes that remind us of some internal structures of the brain such as the hippocampus, amygdala and cingulate gyrus. Blue and red colours respectively mean negative and positive t-values. This shows us that the average measure is smaller in AD than in CTL in some areas that have been widely linked to Alzheimer's disease, as it could be expected. Similar areas present a similar behaviour when using entropy. Conversely, the t-values for kurtosis or skewness present similar patterns to the average or variance measures, although with smaller statistical significance and nega-

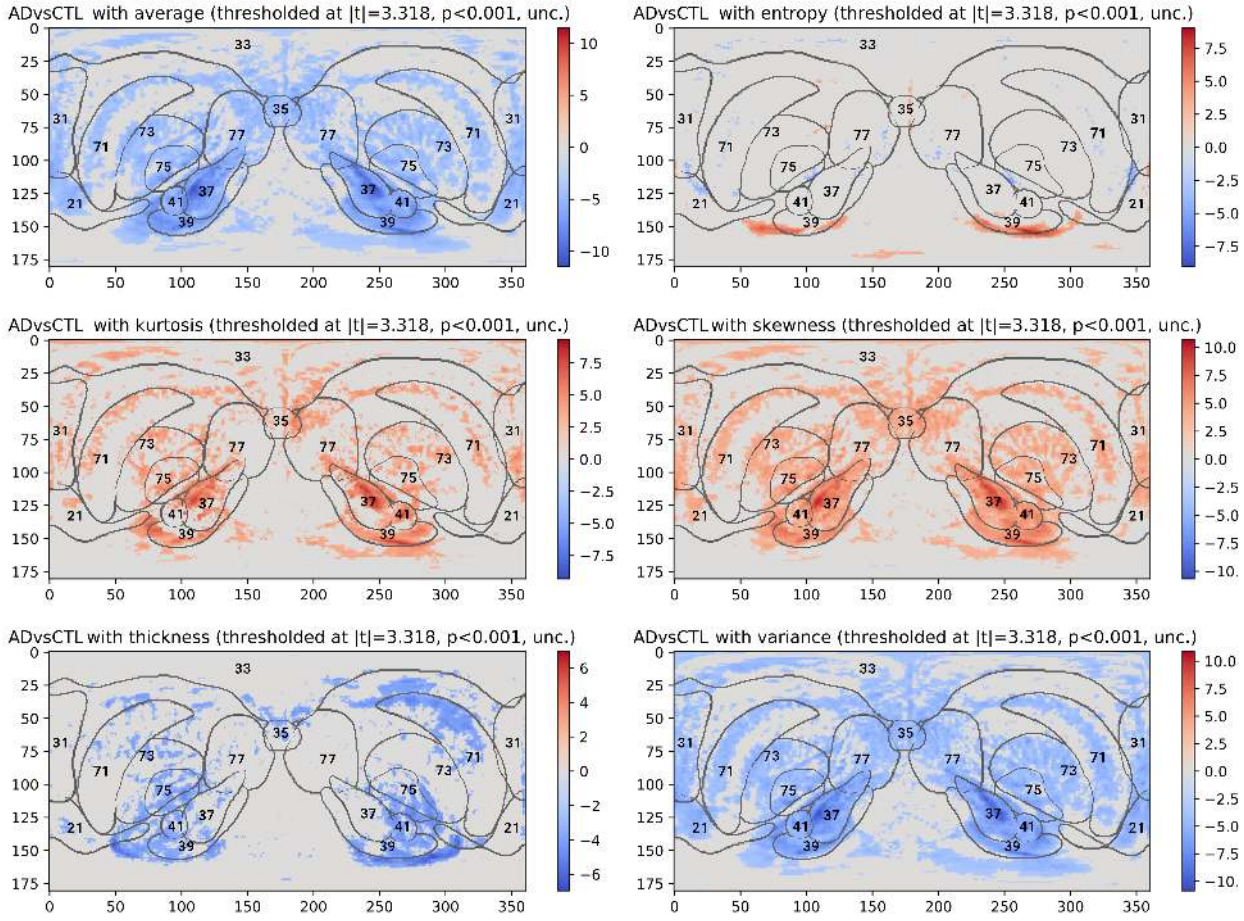

Figure 6: Significant regions according to the uncorrected t-test applied over the AD vs CTL scenario and GM, thresholded at the $p < 0.001$ value. The reference for internal structures is superimposed to the maps.

tive values.

In Figure 6 we show similar information (thresholded significant areas, uncorrected t-test, $p<0.001$) of the WM SBM measures. In this case, the most significant areas are located at the top of the image, which might correspond to the middle part of the cingulate gyrus (33) in the internal reference, and the superior motor area (19) in the external. However, these areas correspond more specifically to the longitudinal fissure, as it can be seen at Figures 2 and 3. Regions at the inferior part of the hippocampus can also be appreciated in the average, skewness, kurtosis and variance maps, and at the posterior part of the caudate nucleus (71).

III.2.2 Correlation with Neuropsychological Tests

In this section we will assess the correlation between each SBM measure and the MMSE and ADAS-13 tests, to check which regions and measures are more related to variations in cognitive ability.

In Figure 8, one general pattern can be described in the SBM's average, kurtosis, skewness and variance measures for GM. In these particular cases, there is a noticeable positive (average and variance) and negative (kurtosis and skewness) correlation between MMSE scores and SBM values at the hippocampus (37), amygdala (41) and parahippocampal gyrus (39). In these cases, the PCC reaches absolute values higher than 0.46. However, two different correlation patterns (smaller, with PCCs around 0.3) appear in entropy and thickness. In these two cases, the maximum correlations are located at the bottom part of the parahippocampal gyrus (39) and, in general, the limits of the temporal lobe. In the case of entropy, we also find some high positive correlations at the frontal superior orbital gyrus (5), occipital superior (49), middle (51), and inferior gyri (53), the angular gyrus (65) and temporal middle gyrus (85), which also could match the thalamus (77) and posterior part of the caudate nucleus (71), globus pallidus (75), the hippocampus (37) and the olfactory bulb (21).

The correlations of the SBM GM-derived measures with ADAS-cog measures are always higher (in some cases, more than 0.1 in absolute value) than the correlations found in MMSE. However, the patterns are extremely similar, but inverse, due to the nature of each kind of test.

Correlations of the WM-derived SBM measures with neuropsychological tests are in all cases smaller, as can be checked at Figure 9 for ADAS-13 (correlations are again higher for ADAS-cog than for MMSE). The patterns are much more related to WM variations, and they can hardly been related to the previous structures. However, most of them show highest PCC values in the superior motor area (19), an area shared between the precentral and postcentral gyrus, including the parietal inferior gyrus (1, 57 and 61 respectively) and, for the thickness measure, the outermost part of the temporal gyrus, near the temporal pole (87).

III.3. Classification Analysis

In this section, we present the results of evaluating the 6 SBM maps for GM and WM tissues under the AD vs CTL and MCI-C vs MCI-S scenarios.

III.3.1 AD vs CTL

Under the first scenario, the classification analysis obtained a performance shown at Table 3. As we can easily see in that table, the best results are obtained by the average measure on the GM tissue, and both average and entropy in the WM tissue. The tendency is that average, entropy and variance obtain similar performance, whereas the skewness, kurtosis, and below all, thickness, are less discriminant between AD and CTL classes.

III.3.2 MCI-C vs MCI-S

Now we will focus on predicting the conversion of MCI subjects. To do so, we will analyse the system when trained and tested with MCI-C and MCI-S. The performance achieved by the different SBM measures is presented at Table 4.

In this case, we can see that the best performing measures are the average (for GM tissue) and variance (for WM tissue). These maps achieve high sensitivity, although smaller than the one obtained when using the VAF approach (see Table 2). Therefore, even when obtaining a significant feature reduction, the performance degrades. This is probably due to the MCI subclasses sparsity in the SBM space and a high overlapping rate between converters and non converters. Therefore, we aim to test whether these two subclasses are better classified when using two more separate clusters, AD and CTL subjects, to train the SVC.

In the second part of Table 4, we provide the classification performance of that very approach, training on AD and CTL subjects and predicting converters by

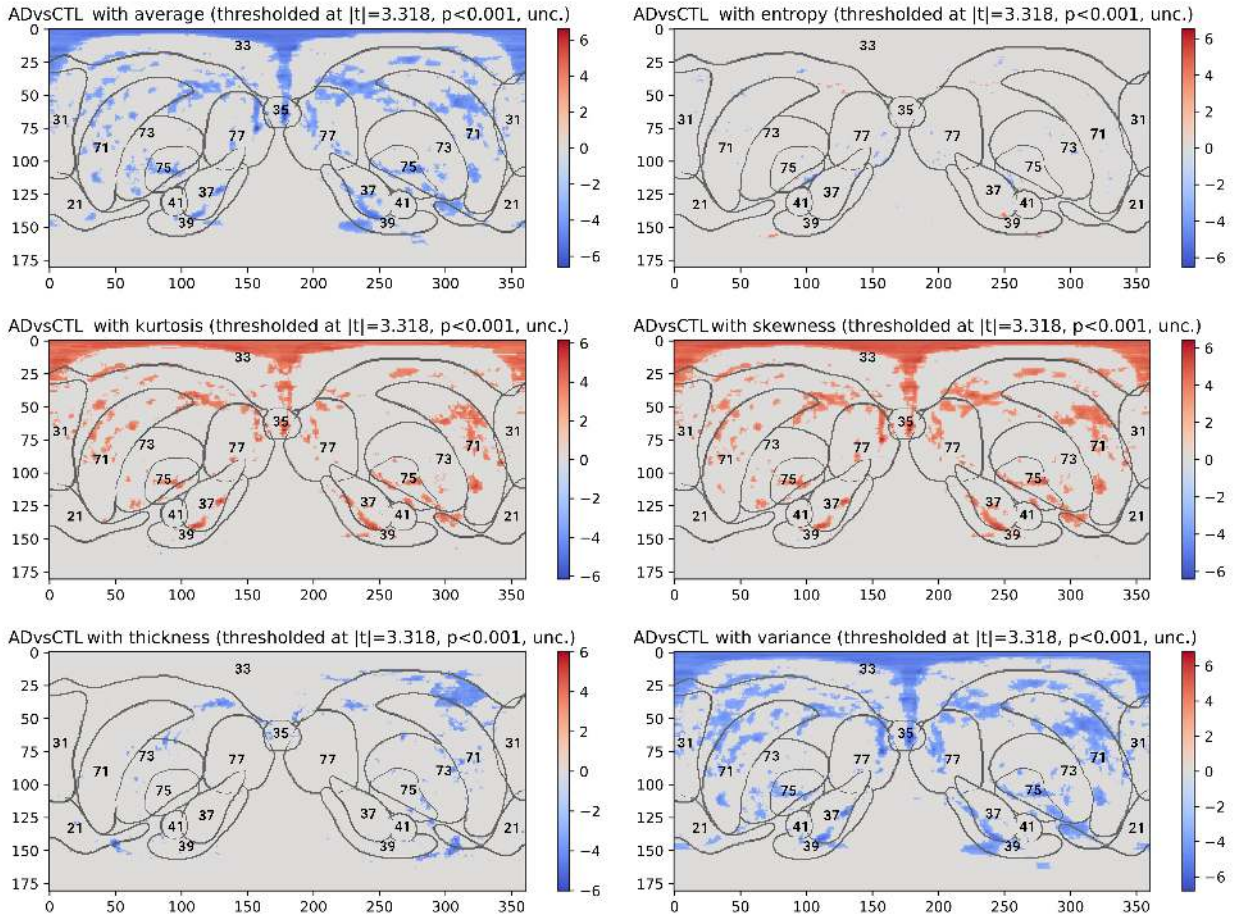

Figure 7: Significant regions according to the uncorrected t-test applied over the **AD vs CTL** scenario and **WM**, thresholded at the $p < 0.001$ value. The reference for **internal** structures is superimposed to the maps.

tissue	measure	acc. [STD]	sens. [STD]	spec. [STD]
GM	**average**	**0.923**[**0.036**]	**0.879**[**0.075**]	**0.958**[**0.077**]
	entropy	0.920[0.054]	0.879[0.095]	0.953[0.089]
	kurtosis	0.895[0.075]	0.852[0.111]	0.929[0.107]
	skewness	0.913[0.059]	0.868[0.102]	0.948[0.094]
	thickness	0.848[0.129]	0.797[0.185]	0.889[0.171]
	variance	0.921[0.047]	0.879[0.093]	0.954[0.085]
WM	average	0.896[0.081]	0.847[0.154]	0.933[0.130]
	entropy	**0.896**[**0.078**]	**0.861**[**0.119**]	**0.923**[**0.115**]
	kurtosis	0.827[0.119]	0.766[0.186]	0.875[0.167]
	skewness	0.857[0.103]	0.807[0.167]	0.897[0.148]
	thickness	0.802[0.130]	0.732[0.198]	0.856[0.181]
	variance	0.891[0.076]	0.853[0.122]	0.921[0.119]

Table 3: Performance of the different SBM measures under the AD vs CTL scenario.

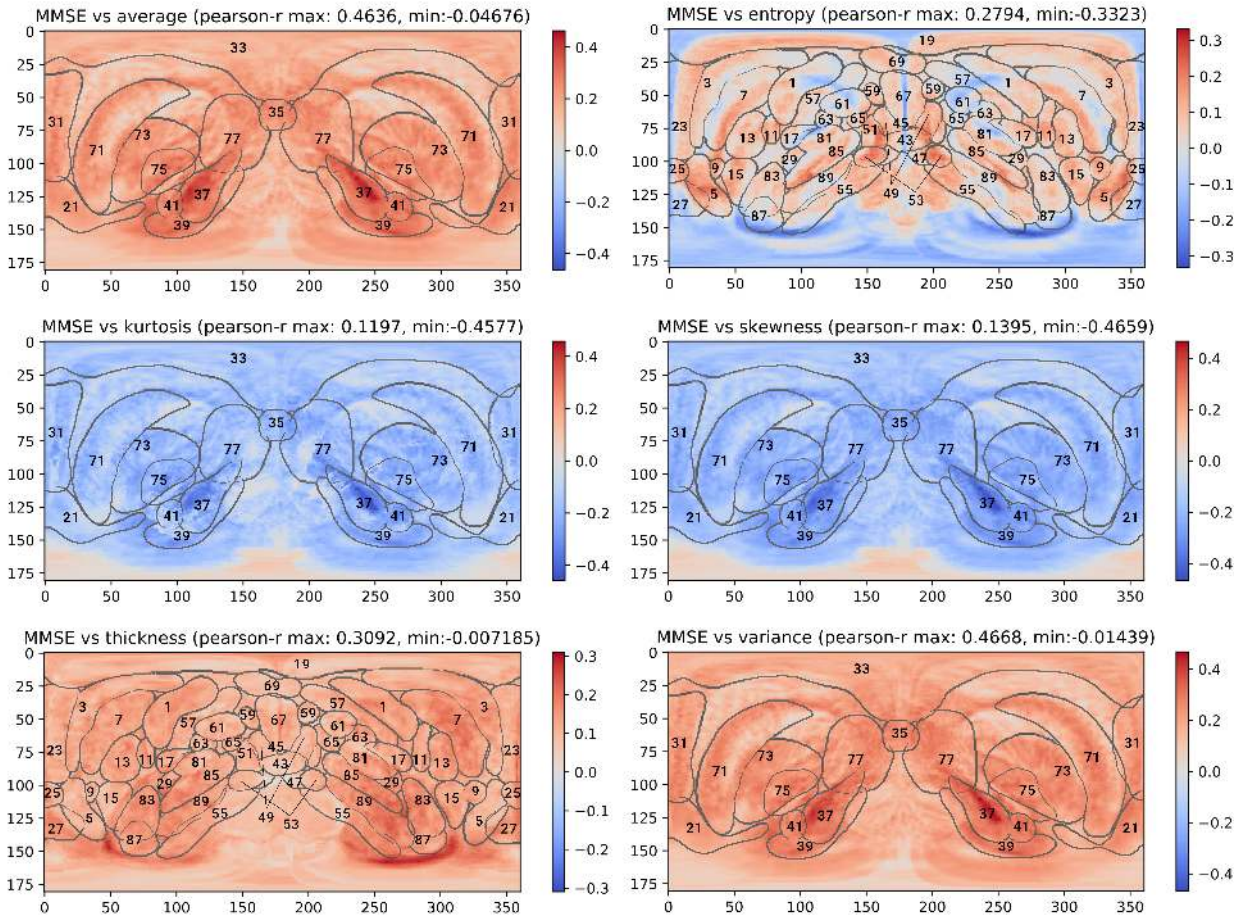

Figure 8: PCC maps computed between the SBM-GM measures and the MMSE. The reference of internal and external structures is superimposed to the figures, depending on the most relevant patterns

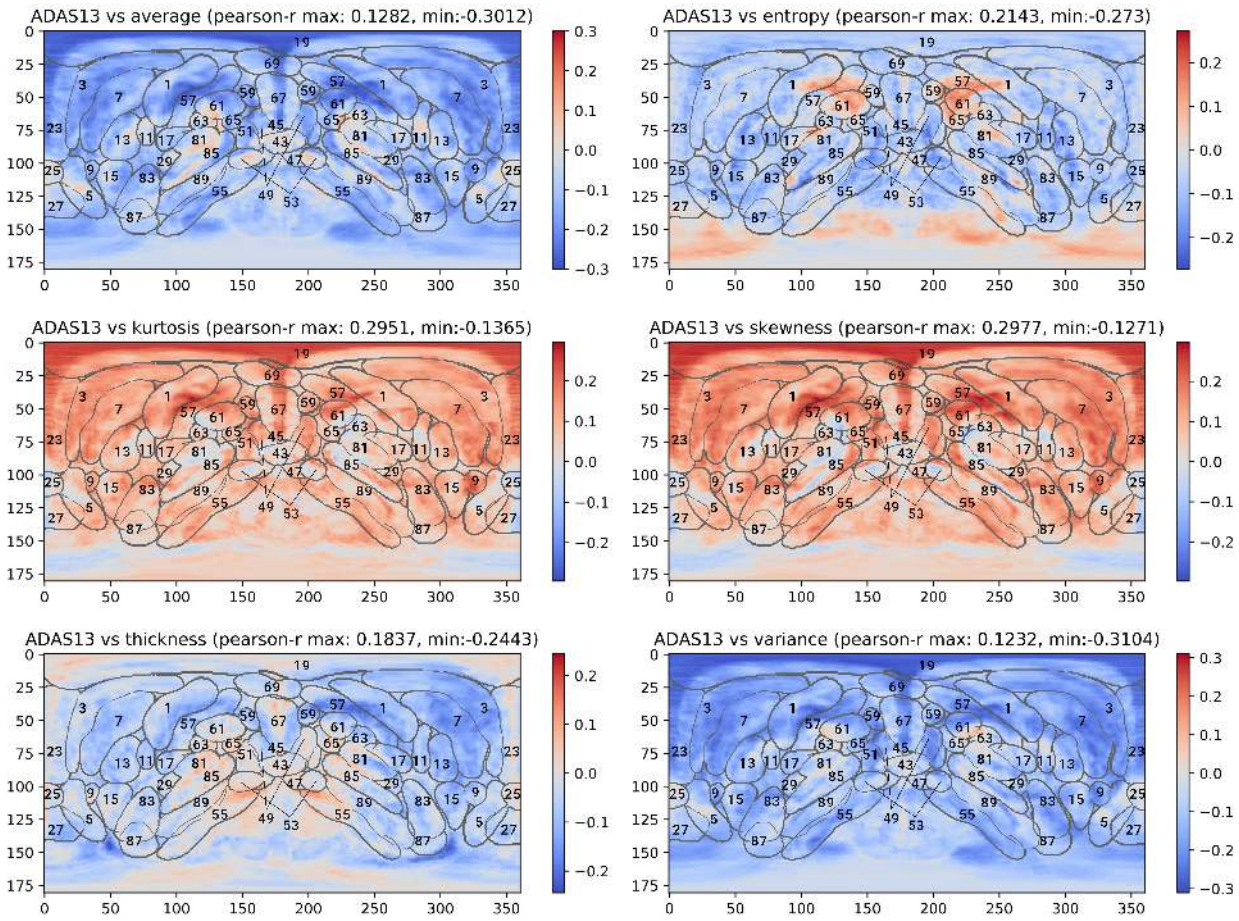

Figure 9: PCC maps computed between the SBM-WM measures and the ADAS-13 (the best scoring of the two ADAS-cog tests).

choosing those more similar to the AD class. We evaluate the different maps when predicting the conversion of MCI subjects by training the classifier with AD and CTL subjects. It is clear that there exist a significant performance increase, of more than 10% in for GM and 5% in WM. In this case, the best performing SBM measure is again average for GM and entropy for WM, outperforming the VAF approach (see Table 2) in this task.

III.4. Regression Analysis

Now we will evaluate how two different regression techniques, LASSO and SVR, can predict neuropsychological test outcomes using SBM maps as as source. The results for this approaches can be found at Table 5.

Regarding the regression model, SVR performs better than LASSO in ADAS-cog and GM. Conversely, LASSO correlates better with MMSE in all cases and ADAS-cog in WM. Of the three tests, the ADAS-13 scores are best modelled, followed by ADAS-11 and, at a long distance, MMSE. The maps that better predict test outcomes are the entropy (in GM and WM) and the variance (for GM when using the SVR). MMSE prediction achieves a poorer performance, with small R^2 values for MMSE, in both GM and WM maps. On the contrary, the variance/entropy maps for GM outperform the same measures in WM by almost 0.2.

IV. Discussion

The main purpose of this work is to test the ability of the SBM maps in two challenging scenarios: predicting the conversion of MCI subjects to dementia at least six months in advance, and predicting neuropsychological tests outcomes from MRI data in order to have another objective measure of cognitive

Tissue	Measure	Trained with MCI-C and MCI-S			Trained with AD and CTL		
		acc. [STD]	sens. [STD]	spec. [STD]	acc. [STD]	spec. [STD]	sens. [STD]
GM	**average**	**0.664**[**0.091**]	**0.700**[**0.149**]	**0.626**[**0.175**]	**0.776**[**0.120**]	**0.826**[**0.182**]	**0.729**[**0.174**]
	entropy	0.644[0.120]	0.695[0.151]	0.593[0.193]	0.731[0.115]	0.837[0.205]	0.633[0.183]
	kurtosis	0.622[0.120]	0.691[0.170]	0.548[0.197]	0.733[0.115]	0.847[0.210]	0.626[0.196]
	skewness	0.638[0.115]	0.700[0.165]	0.573[0.198]	0.739[0.110]	0.854[0.210]	0.632[0.194]
	thickness	0.607[0.120]	0.676[0.177]	0.532[0.201]	0.711[0.122]	0.857[0.235]	0.576[0.218]
	variance	0.646[0.117]	0.686[0.154]	0.604[0.186]	0.746[0.120]	0.802[0.186]	0.693[0.165]
WM	average	0.672[0.149]	0.700[0.207]	0.645[0.231]	0.709[0.146]	0.888[0.235]	0.543[0.200]
	entropy	0.664[0.157]	0.681[0.244]	0.648[0.237]	**0.719**[**0.140**]	**0.862**[**0.218**]	**0.590**[**0.208**]
	kurtosis	0.651[0.156]	0.677[0.215]	0.622[0.226]	0.675[0.151]	0.808[0.232]	0.554[0.224]
	skewness	0.653[0.160]	0.668[0.229]	0.638[0.231]	0.707[0.137]	0.846[0.218]	0.582[0.210]
	thickness	0.641[0.152]	0.671[0.216]	0.607[0.222]	0.672[0.144]	0.796[0.223]	0.560[0.216]
	variance	**0.675**[**0.152**]	**0.679**[**0.234**]	**0.674**[**0.240**]	0.713[0.147]	0.852[0.219]	0.586[0.211]

Table 4: Performance of the different SBM measures under the MCI-C vs MCI-S scenario.

	ADAS11				ADAS13				MMSE			
	LASSO		SVR		LASSO		SVR		LASSO		SVR	
	MSE	R^2	*MSE*	R^2	*MSE*	R^2	*MSE*	R^2	*MSE*	R^2	*MSE*	R^2
average (GM)	49.74	0.263	47.68	0.287	84.73	0.307	72.07	0.412	14.83	0.071	15.62	-0.002
entropy (GM)	**41.04**	**0.392**	39.48	0.414	**67.46**	**0.449**	63.55	0.481	**11.27**	**0.285**	13.17	0.155
kurtosis (GM)	71.95	-0.078	69.69	-0.041	132.6	-0.083	113.9	0.072	19.08	-0.223	38.26	-1.294
skewness (GM)	45.06	0.330	52.15	0.219	79.69	0.353	80.27	0.341	11.71	0.262	15.52	0.014
thickness (GM)	64.18	0.038	52.93	0.211	103.1	0.157	82.74	0.328	16.51	-0.055	15.23	0.026
variance (GM)	58.85	0.127	**39.17**	**0.416**	95.77	0.216	**60.74**	**0.504**	15.97	-0.002	**12.81**	**0.183**
average (WM)	63.72	0.052	59.32	0.104	113.1	0.072	97.54	0.194	15.97	-0.002	15.99	-0.019
entropy (WM)	**48.28**	**0.277**	**48.59**	**0.268**	**77.15**	**0.366**	**81.95**	**0.325**	**11.51**	**0.275**	15.01	0.048
kurtosis (WM)	116.9	-0.754	95.91	-0.437	219.4	-0.805	173.8	-0.428	25.16	-0.598	42.04	-1.715
skewness (WM)	76.16	-0.141	66.33	0.005	139.7	-0.149	114.1	0.062	16.07	-0.019	18.16	-0.153
thickness (WM)	72.64	-0.094	59.74	0.099	119.3	0.019	100.2	0.174	16.31	-0.035	14.45	0.083
variance (WM)	67.33	-0.002	51.73	0.222	119.5	0.019	86.12	0.289	15.97	-0.002	**12.99**	**0.174**

Table 5: Coefficient of determination and MSE of the different models for the three cognitive tests, based on the SBM transformation of GM and WM maps. Best values per test and model are highlighted.

state. This is enhanced by the special characteristics of the SBM mapping, which allows a direct bidimensional visualization of textural changes in the brain.

However, before discussing these two scenarios, we will try to provide intuition about what the different measures mean. In the first place, average, variance, skewness and kurtosis are related to different statistical moments of $V_{\theta,\varphi}$. The average of these intensities is then easy to relate to tissue density, and therefore, a decrease in this measure could be a hint of atrophy in that direction. Note how this occurs in the AD and MCI-C groups at Figure 10, where the mean of all SBM-average maps for each of the four defined groups are displayed. Similarly, the variance of $V_{\theta,\varphi}$ measures the variability in its values. Higher variance could mean higher neurodegeneration, since its values may be more disperse. Skewness and kurtosis are often considered a measure of symmetry and 'peakedness' of the statistical distribution of the intensities in $V_{\theta,\varphi}$. Smaller skewness means that the intensity has decreased, which can also been associated to atrophy. A higher kurtosis is the result of extreme deviations from the mean, which is indicative of more abrupt transitions between grey levels, and therefore, better defined boundaries of GM and WM. Smaller kurtosis can also be related to neurodegeneration.

Thickness is the only morphological measure in this work, and it measures the distance between the first and last voxels in $V_{\theta,\varphi}$ higher than a threshold. It is a rough estimate of tissue thickness, very different from more precise -and complex- cortical thickness measures provided by software such as FreeSurfer

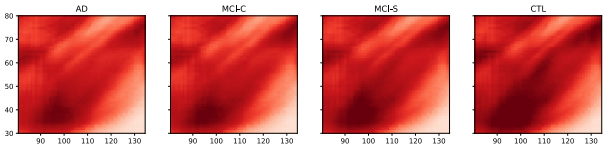

Figure 10: Mean of the SBM-average maps for the AD, MCI-C, MCI-S and CTL groups. Zoom over the hippocampus region.

[12] or the CAT12 toolbox [1]. Finally, entropy comes from information theory, and it measures the 'amount of information' or 'randomness' of $V_{\theta,\varphi}$. In this work, a higher entropy means a more random distribution of the voxels in $V_{\theta,\varphi}$, which may be linked to the structural changes due to the neurodegeneration process.

Now, regarding the first scenario, we presented the regions with more significant differences between AD and CTLs in Section III.2. The highlighted areas in GM, especially in the afterwards higher scoring measures, correspond mainly to the hippocampus, amygdala and parahippocampal gyrus. Differences between MCI-C and MCI-S are also located at these areas, which also project to the external temporal middle gyrus and temporal pole. In WM, there are no significant differences in any SBM measure between MCI-C and MCI-S, which might be due to neurodegeneration affecting first the GM and later progressing to WM [32]. However significant WM differences can be found between AD and CTL in the boundaries of the superior motor area which correspond to the longitudinal fissure, and also some other regions overlapping to the precuneus, cuneus, paracentral lobule and the frontal middle gyrus.

These differences correspond to existing evidence in the literature. The hippocampus is widely regarded as one of the most discriminating structures in structural MRI [5, 6, 8, 35]. Its influence in declarative memory is patent, and many studies have reported atrophy in early AD, along with surrounding structures such as the amygdala and the parahippocampal gyrus. Most studies report early neurodegeneration in MCI in these structures and generally in the temporal lobe [27, 8, 35, 22]. Martinez-Torteya et al. [22] also reported the left medial orbital gyrus and the left inferiolateral remainder of the parietal lobe (area between inferior parietal gyrus and the supramarginal gyrus). The SBM measures are then collecting useful information on neurodegeneration that can be useful for further assessment and visualization.

Regarding the classification performance, we tested four different groups: AD, CTL, MCI-C and MCI-S. In the AD vs CTL performance we achieved high accuracy (around 90% for WM, higher for GM) that may be due to an improvement since our last work. While in [20] we placed the origin of $v_{\theta,\varphi}$ at the geometrical centre of the image, now we place it at the Anterior Commissure, one landmark anatomical position in the literature and one of the points where the two cerebral hemispheres are connected. Thank to this, it may have improved the computation of the SBM measures in different regions of interest, especially internal regions such as the hippocampus or the caudate nucleus.

However, the most relevant classification results are those that predict MCI conversion between 6 and 12 months in advance. The highest performance was obtained when training with AD and CTL subjects, which may be due to a better definition of the separation hyperplane of the SVC by two more distant clusters than the higher-variability MCI subclasses. The reported results are comparable to the state of the art, [16, 10, 5, 23, 27, 26, 6, 22]. Of these studies, which achieved accuracies ranging from 70% to 80%, the best performing approach was the one proposed by Misra et al. [23], which achieved between 75-80% accuracy on a subset of 27 converters and 76 non-converters from the ADNI dataset. Chupin et al. [5] used the larger population, with 210 individuals (76 converters) from ADNI, achieving an accuracy of 64%. Some of these even used histopathological labels, acquired postmortem, instead of clinical labels, which are more heterogeneous and make the classification task more difficult. Our performance results match those achieved by the best methodology in the state of the art, with a larger, more heterogeneous and less prevalent population (70 converters + 64 non converters), which is key for comparison.

Of all SBM measures used in this article, the average, variance and entropy measures achieved similar performance. Particularly, average worked very well with segmented GM maps, whereas the entropy always performed better in the WM. Thickness yielded the poorest performance, perhaps due to the lack of relevant features in areas of interests such as the hippocampus.

In the second scenario, the PCC maps show the areas that are highly correlated with different neuropsychological tests. The main impression is that the ADAS-cog scores (especially the ADAS-13) achieve higher correlations with the MRI data than the MMSE, suggesting that these measures are much more specific of AD progression and cognitive decline. This is

also supported by current literature [15, 34], where some authors claim that non-specific neuropsychological scores may be a source of false positives, especially in MCI.

In GM, correlations with the ADAS-13 test outcomes scored higher than 0.5 in areas such as the hippocampus and parts of the parahippocampal gyrus. This was repeated in the average, variance, skewness and kurtosis measures. Entropy and thickness measures revealed different patterns, with maximum correlations in the lower boundary of the temporal lobe. As for the WM, the correlations were smaller (maximum values around 0.3), with more correlated areas in the longitudinal fissure and, only in the case of entropy, the occipital middle gyrus, the parietal inferior gyrus and the junction between the temporal middle and inferior gyri.

The performance of the regression methods is displayed at Table 5. The reader may note the large differences between the MSE in the ADAS-cog tests and the MMSE, but this is related to a much higher variability in the values (ADAS-13 ranges from 0 to 63 in our database, and ADAS-11 from 0 to 48) compared to the MMSE (ranges from 14 to 30). See Table 1 for more information on the demographics of the dataset. The R^2, however, takes into account this variability, yielding a more consistent measure of the performance, and that is why we will focus on it throughout this section.

Two main properties can be inferred from Table 5's data. First, the differences in R^2 scores stress again the usefulness of the ADAS-cog against the MMSE in measuring Alzheimer's progression. Second, They show that the SVR performs better than LASSO in predicting test outcomes for ADAS-cog in GM. Since LASSO internally focuses on a small number of features, it may be an indication that there are moderately correlated covariates in the maps, which would eventually degrade its performance [7]. Then, SVR is a more adequate choice in this case. Conversely, LASSO outperforms SVR in modelling MMSE, however its performance is smaller than with the ADAS-cog. In WM, our regression techniques can find even less evidence to predict neuropsychological tests, which adds support to the fact that GM neurodegeneration is a better predictor of cognitive state.

The maps with higher performance in predicting neuropsychological tests are entropy and variance. This differs with the largest PCCs computed for each $v_{\theta,\varphi}$ in the maps, where average, kurtosis, skewness and variance had the largest correlations. However, PCCs were obtained for each individual SBM value at the (θ, φ) position, where the regression methods use all values in the maps to create a linear model that predicts the neuropsychological outcomes. Therefore it is possible that entropy, where individual PCCs were relatively smaller, contains relevant -and different- information in more areas than the other maps, and those values can be used to inform a more accurate model of the test. When looking at the PCC maps for the SBM-entropy, large negative and positive correlations were found in GM (in contrast to all other measures), including negative PCCs at the lower boundary of the temporal lobe and positive at the angular gyrus, thalamus, occipital gyrus, caudate nucleus, etc., that have also been found in functional imaging [21]. The pattern in WM pattern is similar, which may be the reason why the SBM-entropy achieves best performance in regression.

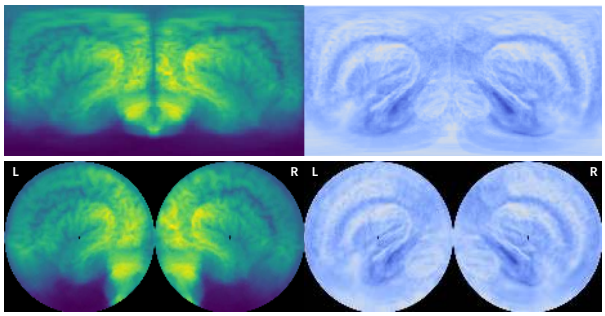

Figure 11: Comparison between the equirectangular projection for two SBM examples (an average map and the PCC maps computed at Sec. III.2.2) and the stereographic projection, currently in development.

The SBM mapping, as any other technique intended to visualize three-dimensional volumes in two dimensions, is subject to deformations due to the projections. Our choice for SBM, given its simplicity, was the equirectangular projection, also known as *plate carrée* projection [29]. However, it is neither equal area nor conformal, introducing distortions as the elevation θ increases. Other projections, for example the stereographic projection [29] (see Fig. 11 for comparisons), might seem more convenient for visualization. This last projection is conformal and therefore preserves angular relationships, yielding a more brain-like, intuitive visualization of the SBM maps. We plan to include this approach in future releases of the python `mapBrain` package, which contains SBM.

In summary, the SBM offers a series of bidimensional maps that provide a significant feature reduction along with a visual aid that could be useful to locate differences, in combination with either hypoth-

esis testing or correlation analysis. We have proven that a classifier trained with SBM average maps from AD and CTL subjects can effectively predict conversion of MCI in the session immediately previous to their reported conversion session (that is, in all cases, between 6 and 12 months in advance), with a 77% accuracy and 73% sensitivity. And ultimately, we demonstrated that these maps can be used to predict scores that match the outcomes of clinical tests, providing an objective replication tool based on imaging data.

V. Conclusions

In this work, we propose the application of a Spherical Brain Mapping (SBM) of Magnetic Resonance Imaging (MRI) in two challenging scenarios involving Alzheimer's Disease (AD): predicting the conversion of MCI subjects to dementia at least six months in advance, and predicting neuropsychological tests outcomes from MRI data. These two classification and regression scenarios are tested using Support Vector Machines and LASSO, providing numerical evidence of their performance. Moreover, we also analyse visual evidence on the affected regions via hypothesis testing (for differences between groups) and correlation coefficient (for correlation with test outcomes).

The SBM maps provide a significant feature reduction over the million-voxel MRI images, while achieving a state-of-the-art performance (77% accuracy) in the prediction of MCI conversion more than 6 months in advance. The best prediction is obtained with a classifier trained with AD and control (CTL) classes which, thanks to being separate clusters, define a better separation hyperplane. Significant differences between maps have been found at the hippocampus, parahippocampal gyrus and more generally the temporal lobe, all of which have a proven relationship with AD progression.

For its part, the relationship between some of the SBM measures in GM and the outcomes of neuropsychological tests has also been proven. The highest performance of this regression analysis is achieved when predicting the ADAS-cog, supporting existing evidence that this test is more indicative of the disease stage than the MMSE. R^2 scores up to 0.504 were obtained when predicting ADAS-13 with Support Vector Regression on the SBM-variance maps. The SBM average and variance measures are also noticeably correlated with this test (pearson-r higher than 0.5). A visual analysis of the pearson-r reveals the utility of the bidimensional representation in identifying changes in texture along the brain. Regions typically related with AD, achieve highest correlation rates, but the most persistent area is the hippocampus.

In summary, the SBM offers a series of bidimensional maps that provide a significant feature reduction along with a visual aid that could be useful to locate differences, in combination with either hypothesis testing or correlation analysis. These maps keep relevant textural information that allows a system to predict MCI conversion more than six months in advance. New projections to enhance visualization are currently being explored, in order to provide a more intuitive insight of the brain structure.

Acknowledgements

This work was partly supported by the MINECO/ FEDER under the TEC2015-64718-R project, the Consejería de Economía, Innovación, Ciencia y Empleo (Junta de Andalucía, Spain) under the Excellence Project P11-TIC- 7103 and the Salvador de Madariaga Mobility Grants 2017.

Data collection and sharing for this project was funded by the Alzheimer's Disease Neuroimaging Initiative (ADNI) (National Institutes of Health Grant U01 AG024904) and DOD ADNI (Department of Defense award number W81XWH-12-2-0012). ADNI is funded by the National Institute on Aging, the National Institute of Biomedical Imaging and Bioengineering, and through generous contributions from the following: AbbVie, Alzheimer's Association; Alzheimer's Drug Discovery Foundation; Araclon Biotech; BioClinica, Inc.; Biogen; Bristol-Myers Squibb Company; CereSpir, Inc.; Cogstate; Eisai Inc.; Elan Pharmaceuticals, Inc.; Eli Lilly and Company; EuroImmun; F. Hoffmann-La Roche Ltd and its affiliated company Genentech, Inc.; Fujirebio; GE Healthcare; IXICO Ltd.; Janssen Alzheimer Immunotherapy Research & Development, LLC.; Johnson & Johnson Pharmaceutical Research & Development LLC.; Lumosity; Lundbeck; Merck & Co., Inc.; Meso Scale Diagnostics, LLC.; NeuroRx Research; Neurotrack Technologies; Novartis Pharmaceuticals Corporation; Pfizer Inc.; Piramal Imaging; Servier; Takeda Pharmaceutical Company; and Transition Therapeutics. The Canadian Institutes of Health Research is providing funds to support ADNI clinical sites in Canada. Private sector contributions are facilitated by the Foundation for the National Institutes of Health (`www.fnih.org`). The grantee organization is the Northern California Insti-

tute for Research and Education, and the study is coordinated by the Alzheimer's Therapeutic Research Institute at the University of Southern California. ADNI data are disseminated by the Laboratory for Neuro Imaging at the University of Southern California.

Conflict of Interest

The authors have no conflict of interest to report.

References

[1] Adaszewski, S., Dukart, J., Kherif, F., Frackowiak, R., Draganski, B., and , A. D. N. I. (2013). How early can we predict Alzheimer's disease using computational anatomy? *Neurobiology of Aging*, 34(12):2815–2826.

[2] Alzheimer's Association (2016). 2016 Alzheimer's disease facts and figures. *Alzheimer's & Dementia*, 12(4):459–509.

[3] Cano, S. J., Posner, H. B., Moline, M. L., Hurt, S. W., Swartz, J., Hsu, T., and Hobart, J. C. (2010). The ADAS-cog in Alzheimer's disease clinical trials: psychometric evaluation of the sum and its parts. *Journal of Neurology, Neurosurgery & Psychiatry*, 81(12):1363–1368.

[4] Cherkassky, V. and Ma, Y. (2004). Practical selection of SVM parameters and noise estimation for SVM regression. *Neural networks*, 17(1):113–126.

[5] Chupin, M., Gérardin, E., Cuingnet, R., Boutet, C., Lemieux, L., Lehéricy, S., Benali, H., Garnero, L., Colliot, O., Initiative, A. D. N., et al. (2009). Fully automatic hippocampus segmentation and classification in Alzheimer's disease and mild cognitive impairment applied on data from ADNI. *Hippocampus*, 19(6):579.

[6] Costafreda, S. G., Dinov, I. D., Tu, Z., Shi, Y., Liu, C.-Y., Kloszewska, I., Mecocci, P., Soininen, H., Tsolaki, M., Vellas, B., et al. (2011). Automated hippocampal shape analysis predicts the onset of dementia in mild cognitive impairment. *Neuroimage*, 56(1):212–219.

[7] Dalalyan, A. S., Hebiri, M., Lederer, J., et al. (2017). On the prediction performance of the lasso. *Bernoulli*, 23(1):552–581.

[8] Desikan, R. S., Cabral, H. J., Hess, C. P., Dillon, W. P., Glastonbury, C. M., Weiner, M. W., Schmansky, N. J., Greve, D. N., Salat, D. H., Buckner, R. L., et al. (2009). Automated MRI measures identify individuals with mild cognitive impairment and Alzheimer's disease. *Brain*, page awp123.

[9] Duchesne, S., Caroli, A., Geroldi, C., Frisoni, G. B., and Collins, D. L. (2005). Predicting clinical variable from MRI features: Application to MMSE in MCI. In *Lecture Notes in Computer Science*, pages 392–399. Springer Berlin Heidelberg.

[10] Fan, Y., Resnick, S. M., Wu, X., and Davatzikos, C. (2008). Structural and functional biomarkers of prodromal Alzheimer's disease: A high-dimensional pattern classification study. *Neuroimage*, 41(2):277–285.

[11] Fay, M. P. and Proschan, M. A. (2010). Wilcoxon-Mann-Whitney or t-test? On assumptions for hypothesis tests and multiple interpretations of decision rules. *Statistics Surveys*, 4:1–39.

[12] Fischl, B. and Dale, A. M. (2000). Measuring the thickness of the human cerebral cortex from magnetic resonance images. *Proceedings of the National Academy of Sciences*, 97(20):11050–11055.

[13] Friston, K., Ashburner, J., Kiebel, S., Nichols, T., and Penny, W. (2007). *Statistical Parametric Mapping: The Analysis of Functional Brain Images*. Academic Press.

[14] Khedher, L., Ramírez, J., Górriz, J., Brahim, A., and Segovia, F. (2015). Early diagnosis of Alzheimer's disease based on partial least squares, principal component analysis and support vector machine using segmented MRI images. *Neurocomputing*, 151:139–150.

[15] Klekociuk, S. Z., Summers, J. J., Vickers, J. C., and Summers, M. J. (2014). Reducing false positive diagnoses in mild cognitive impairment: the importance of comprehensive neuropsychological assessment. *European Journal of Neurology*, 21(10):1330–e83.

[16] Klöppel, S., Stonnington, C. M., Chu, C., Draganski, B., Scahill, R. I., Rohrer, J. D., Fox, N. C., Jack, C. R., Ashburner, J., and Frackowiak, R. S. (2008). Automatic classification of MR scans in Alzheimer's disease. *Brain*, 131(3):681–689.

[17] Kohavi, R. and John, G. H. (1995). Wrappers for Feature Subset Selection.

[18] Martinez-Murcia, F., Górriz, J., and Ramírez, J. (2016a). *Computer Aided Diagnosis in Neuroimaging*, chapter 7, pages 137–160. InTech, 1 edition.

[19] Martínez-Murcia, F., Górriz, J., Ramírez, J., Moreno-Caballero, M., Gómez-Río, M., Parkinson's Progression Markers Initiative, et al. (2014). Parametrization of textural patterns in 123I-ioflupane imaging for the automatic detection of parkinsonism. *Medical physics*, 41(1):012502.

[20] Martinez-Murcia, F., Górriz, J., Ramírez, J., Ortiz, A., and for the Alzheimers Disease Neuroimaging Initiative (2016b). A spherical brain mapping of MR images for the detection of Alzheimer's disease. *Current Alzheimer Research*, 13(5):575–588.

[21] Martinez-Murcia, F. J., Górriz, J. M., Ramírez, J., Illán, I. A., Segovia, F., Castillo-Barnes, D., and Salas-Gonzalez, D. (2017). Functional brain imaging synthesis based on image decomposition and kernel modeling: Application to neurodegenerative diseases. *Frontiers in Neuroinformatics*, 11.

[22] Martinez-Torteya, A., Rodriguez-Rojas, J., Celaya-Padilla, J. M., Galván-Tejada, J. I., Treviño, V., and Tamez-Peña, J. (2014). Magnetization-prepared rapid acquisition with gradient echo magnetic resonance imaging signal and texture features for the prediction of mild cognitive impairment to Alzheimer's disease progression. *Journal of Medical Imaging*, 1(3):031005–031005.

[23] Misra, C., Fan, Y., and Davatzikos, C. (2009). Baseline and longitudinal patterns of brain atrophy in MCI patients, and their use in prediction of short-term conversion to AD: Results from ADNI. *Neuroimage*, 44(4):1415–1422.

[24] Ortiz, A., Górriz, J. M., Ramírez, J., and Martínez-Murcia, F. J. (2013). LVQ-SVM based CAD tool applied to structural MRI for the diagnosis of the Alzheimer's disease. *Pattern Recognition Letters*, 34(14):1725–1733.

[25] Pedregosa, F., Varoquaux, G., Gramfort, A., Michel, V., Thirion, B., Grisel, O., Blondel, M., Prettenhofer, P., Weiss, R., Dubourg, V., Vanderplas, J., Passos, A., Cournapeau, D., Brucher, M., Perrot, M., and Duchesnay, E. (2011). Scikit-learn: Machine learning in Python. *Journal of Machine Learning Research*, 12:2825–2830.

[26] Plant, C., Teipel, S. J., Oswald, A., Böhm, C., Meindl, T., Mourao-Miranda, J., Bokde, A. W., Hampel, H., and Ewers, M. (2010). Automated detection of brain atrophy patterns based on MRI for the prediction of Alzheimer's disease. *Neuroimage*, 50(1):162–174.

[27] Querbes, O., Aubry, F., Pariente, J., Lotterie, J.-A., Démonet, J.-F., Duret, V., Puel, M., Berry, I., Fort, J.-C., Celsis, P., et al. (2009). Early diagnosis of Alzheimer's disease using cortical thickness: impact of cognitive reserve. *Brain*, 132(8):2036–2047.

[28] Segovia, F., Górriz, J. M., Ramírez, J., Salas-González, D., Álvarez, I., López, M., Chaves, R., and Padilla, P. (2010). Classification of functional brain images using a GMM-based multi-variate approach. *Neuroscience Letters*, 474:58–72.

[29] Snyder, J. P. (1993). Flattening the earth: 2000 years of map projections.

[30] Stoeckel, J., Ayache, N., Malandain, G., Koulibaly, P. M., Ebmeier, K. P., and Darcourt, J. (2004). Automatic Classification of SPECT Images of Alzheimer's Disease Patients and Control Subjects. In *Medical Image Computing and Computer-Assisted Intervention - MICCAI*, volume 3217 of *Lecture Notes in Computer Science*, pages 654–662. Springer.

[31] Tzourio-Mazoyer, N., Landeau, B., Papathanassiou, D., Crivello, F., Etard, O., Delcroix, N., Mazoyer, B., and Joliot, M. (2002). Automated anatomical labeling of activations in SPM using a macroscopic anatomical parcellation of the MNI MRI single-subject brain. *Neuroimage*, 15(1):273–289.

[32] Villain, N., Fouquet, M., Baron, J.-C., Mézenge, F., Landeau, B., de La Sayette, V., Viader, F., Eustache, F., Desgranges, B., and Chételat, G. (2010). Sequential relationships between grey matter and white matter atrophy and brain metabolic abnormalities in early Alzheimer's disease. *Brain*, 133(11):3301–3314.

[33] Weiner, M. W., Veitch, D. P., Aisen, P. S., Beckett, L. A., Cairns, N. J., Green, R. C., Harvey, D., Jack, C. R., Jagust, W., Liu, E., Morris, J. C., Petersen, R. C., Saykin, A. J., Schmidt, M. E., Shaw, L., Siuciak, J. A., Soares, H., Toga, A. W., and Trojanowski, J. Q. (2012). The Alzheimer's Disease Neuroimaging Initiative: a review of papers published since its inception. *Alzheimer's & dementia: the journal of the*

Alzheimer's Association, 8(1 Suppl):S1–68. PMID: 22047634.

[34] Weissberger, G. H., Strong, J. V., Stefanidis, K. B., Summers, M. J., Bondi, M. W., and Stricker, N. H. (2017). Diagnostic accuracy of memory measures in Alzheimer's dementia and mild cognitive impairment: a systematic review and meta-analysis. *Neuropsychology Review*.

[35] Zhang, J., Yu, C., Jiang, G., Liu, W., and Tong, L. (2012). 3D texture analysis on MRI images of Alzheimer's disease. *Brain imaging and behavior*, 6(1):61–69.

[36] Zhang, Y., Guo, W., and Ray, S. (2016). On the consistency of feature selection with lasso for non-linear targets. In *International Conference on Machine Learning*, pages 183–191.

A. Supplementary Material

A.1. Differences Between Classes

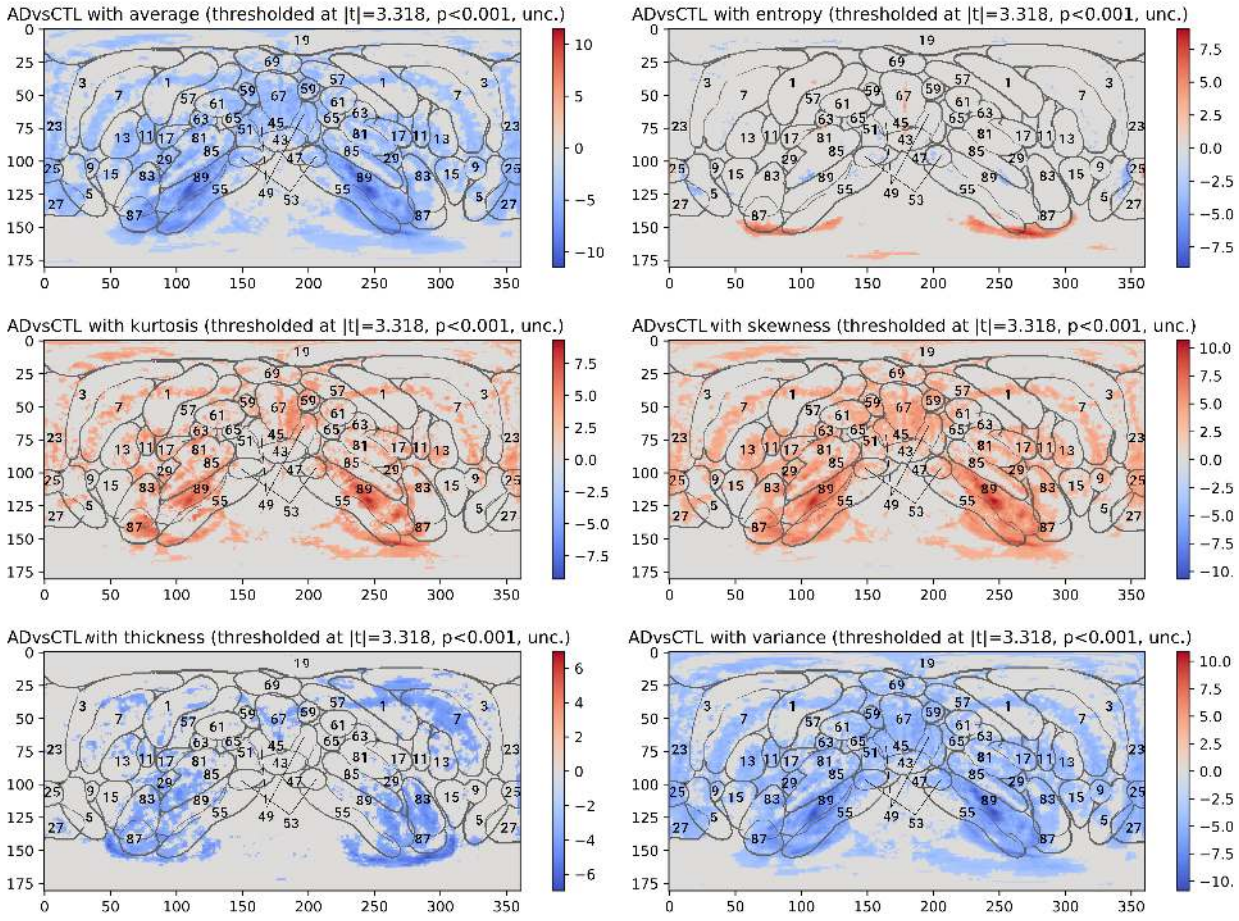

Figure 12: Significant regions according to the uncorrected t-test applied over the **AD vs CTL** scenario and **GM**, thresholded at the $p < 0.001$ value. The reference for **external** structures is superimposed to the maps.

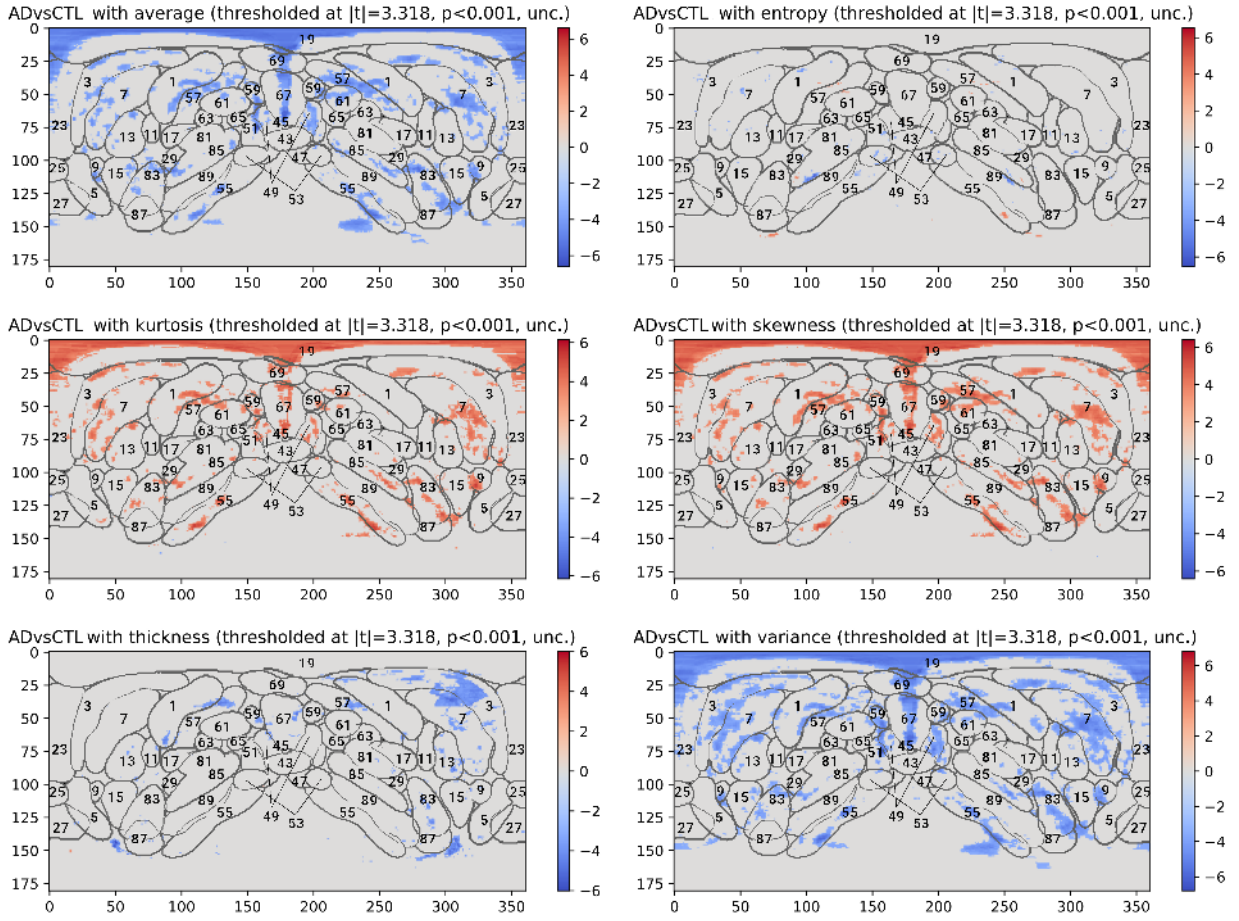

Figure 13: Significant regions according to the uncorrected t-test applied over the **AD vs CTL** scenario and **WM**, thresholded at the $p < 0.001$ value. The reference for **external** structures is superimposed to the maps.

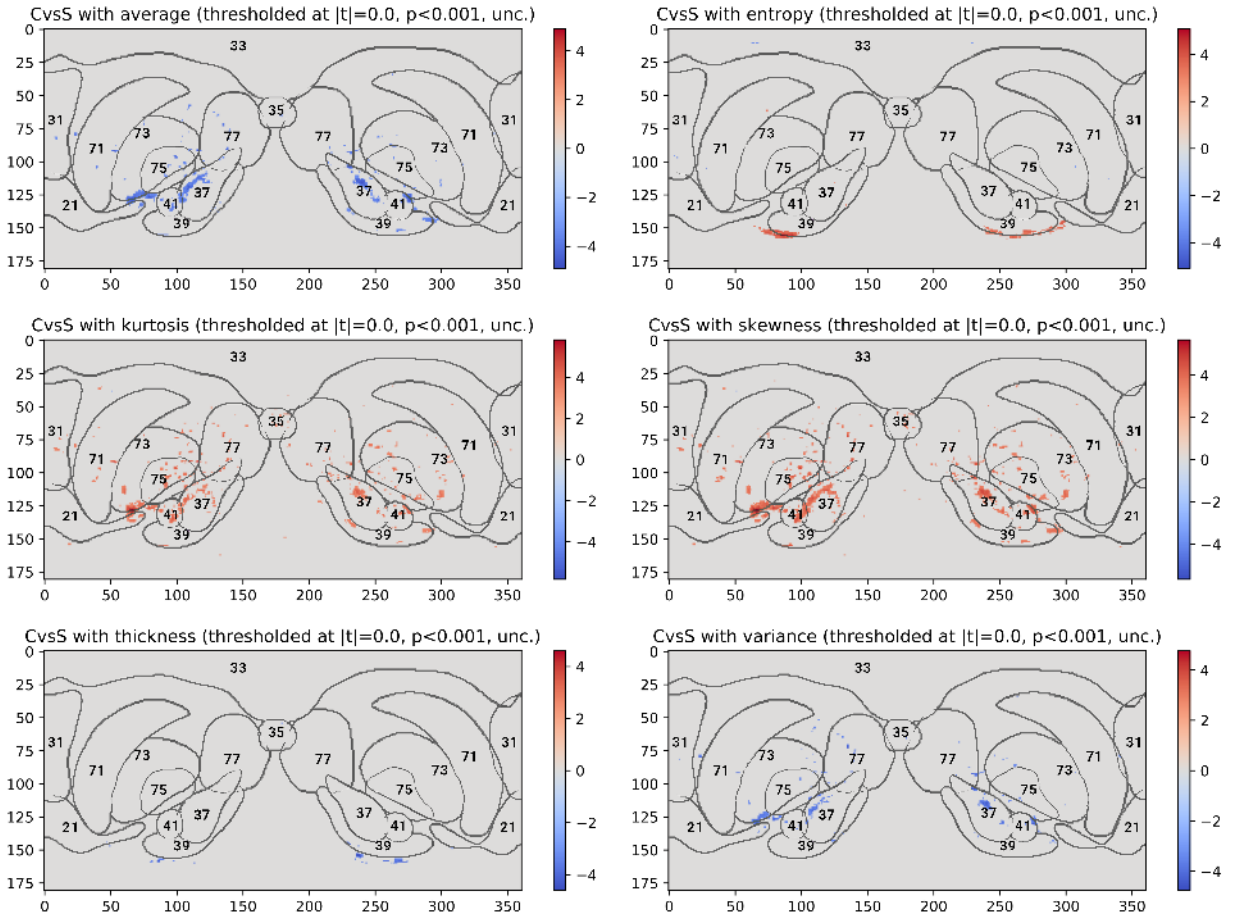

Figure 14: Significant regions according to the uncorrected t-test applied over the **MCI-C vs MCI-S** scenario and **GM**, thresholded at the $p < 0.001$ value. The reference for **internal** structures is superimposed to the maps.

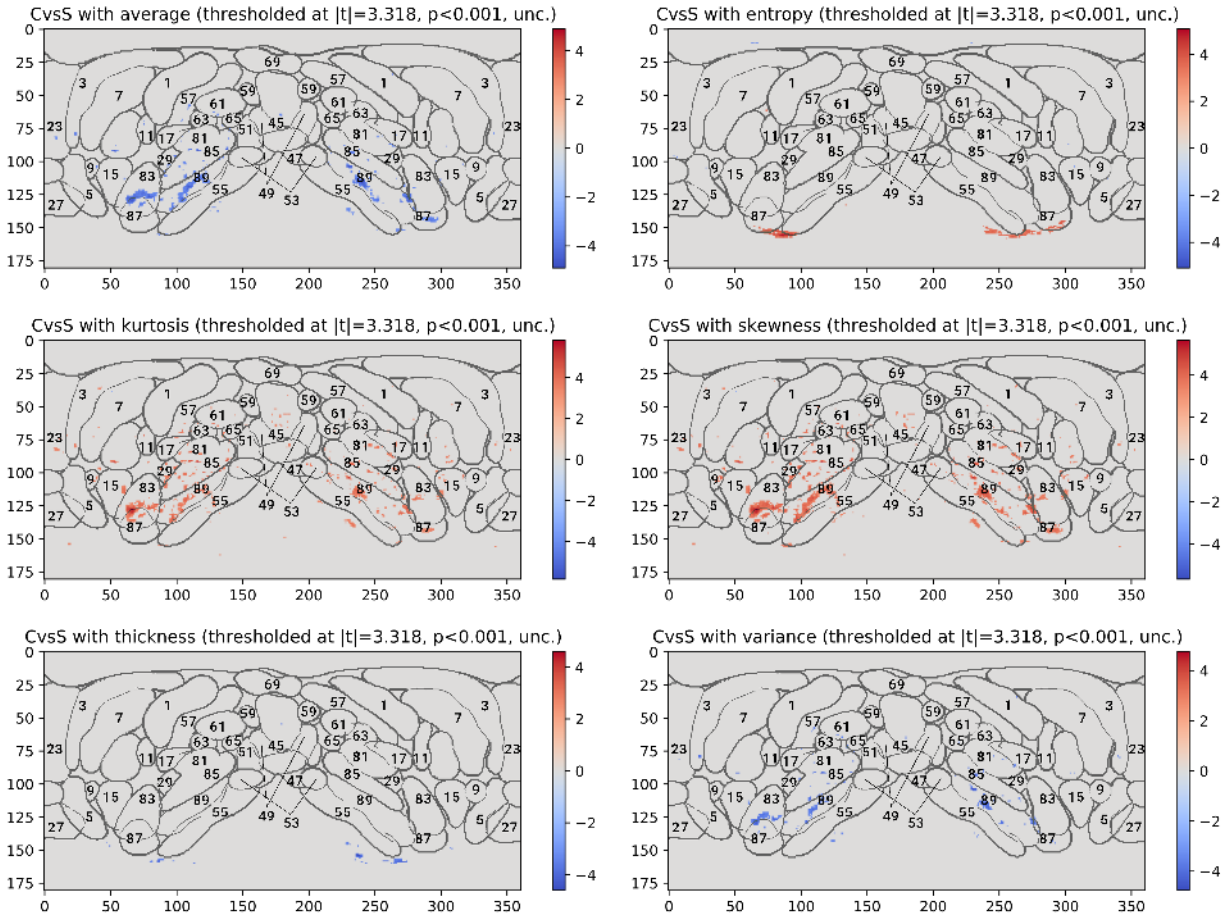

Figure 15: Significant regions according to the uncorrected t-test applied over the **MCI-C vs MCI-S** scenario and **GM**, thresholded at the $p < 0.001$ value. The reference for **external** structures is superimposed to the maps.

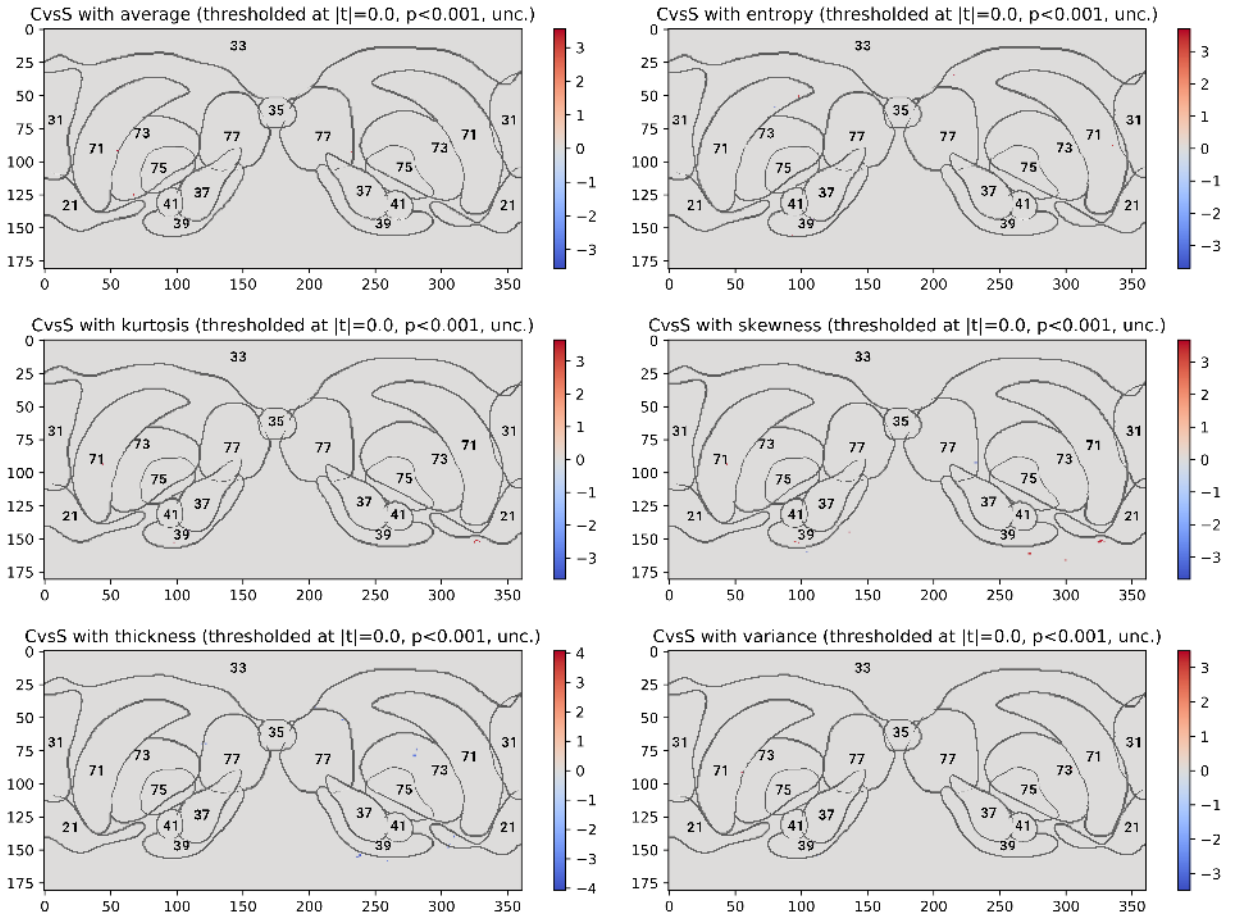

Figure 16: Significant regions according to the uncorrected t-test applied over the **MCI-C vs MCI-S** scenario and **WM**, thresholded at the $p < 0.001$ value. The reference for **internal** structures is superimposed to the maps.

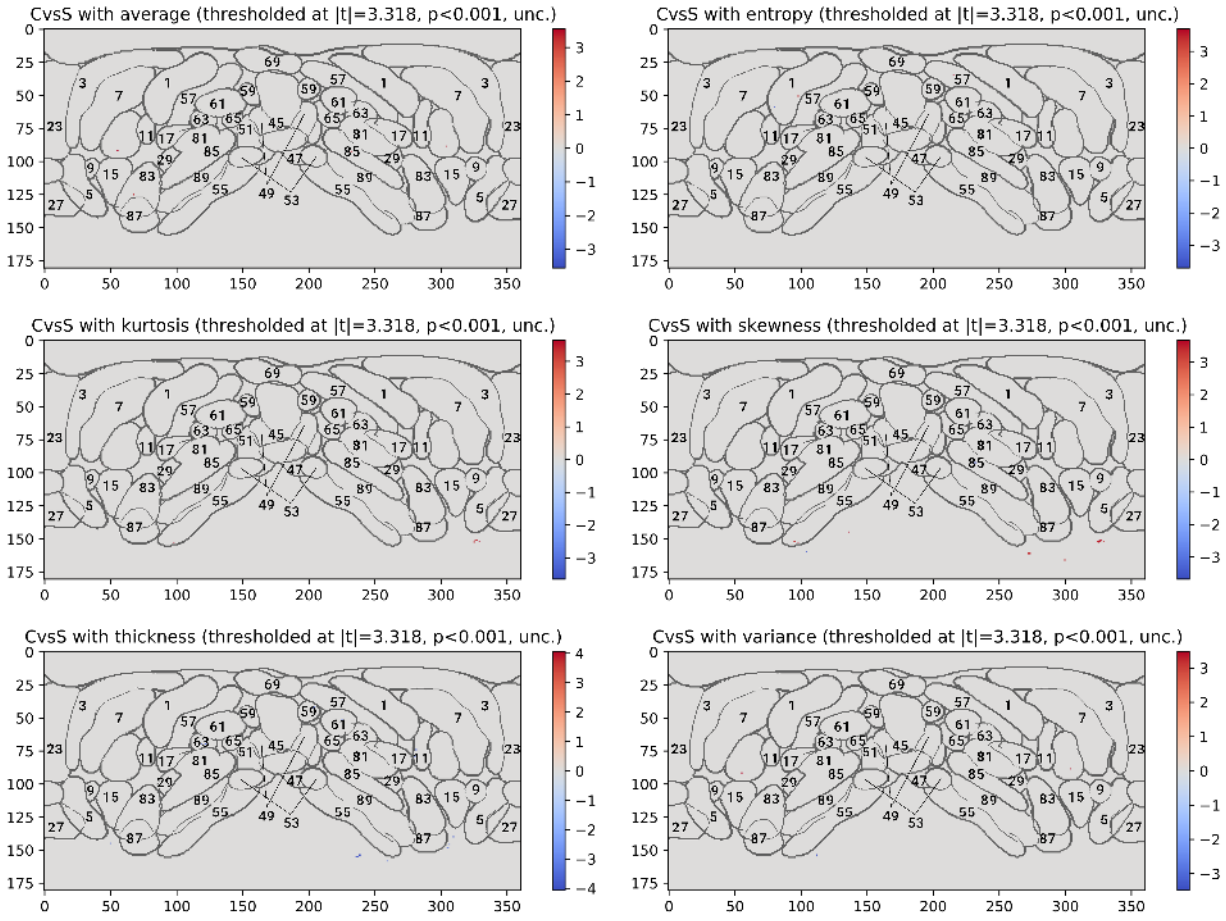

Figure 17: Significant regions according to the uncorrected t-test applied over the **MCI-C vs MCI-S** scenario and **WM**, thresholded at the $p < 0.001$ value. The reference for **external** structures is superimposed to the maps.

A.2. Correlation with Neuropsychological Tests

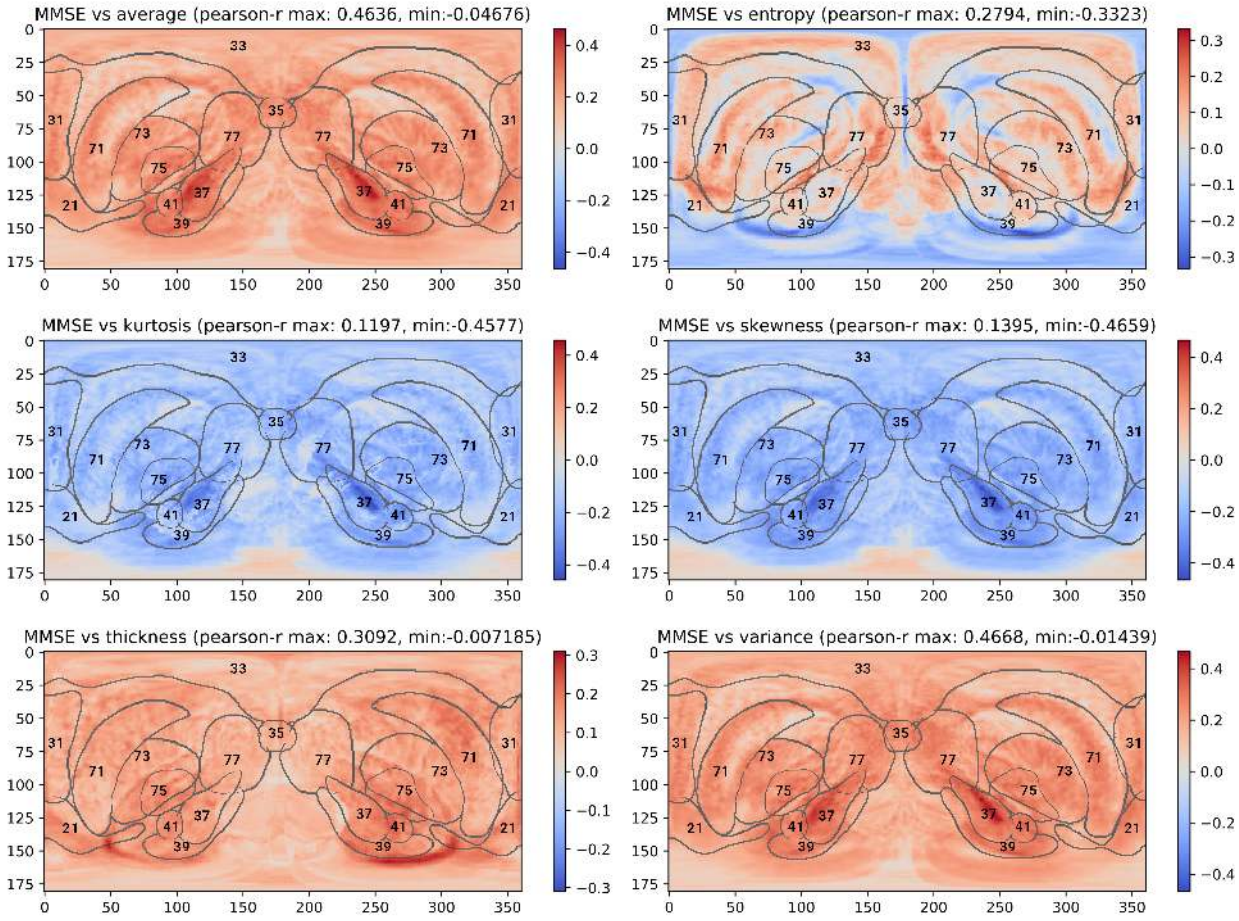

Figure 18: PCC maps computed between the SBM measures for **GM** and the **MMSE**. The reference of **internal** structures is superimposed to the figures.

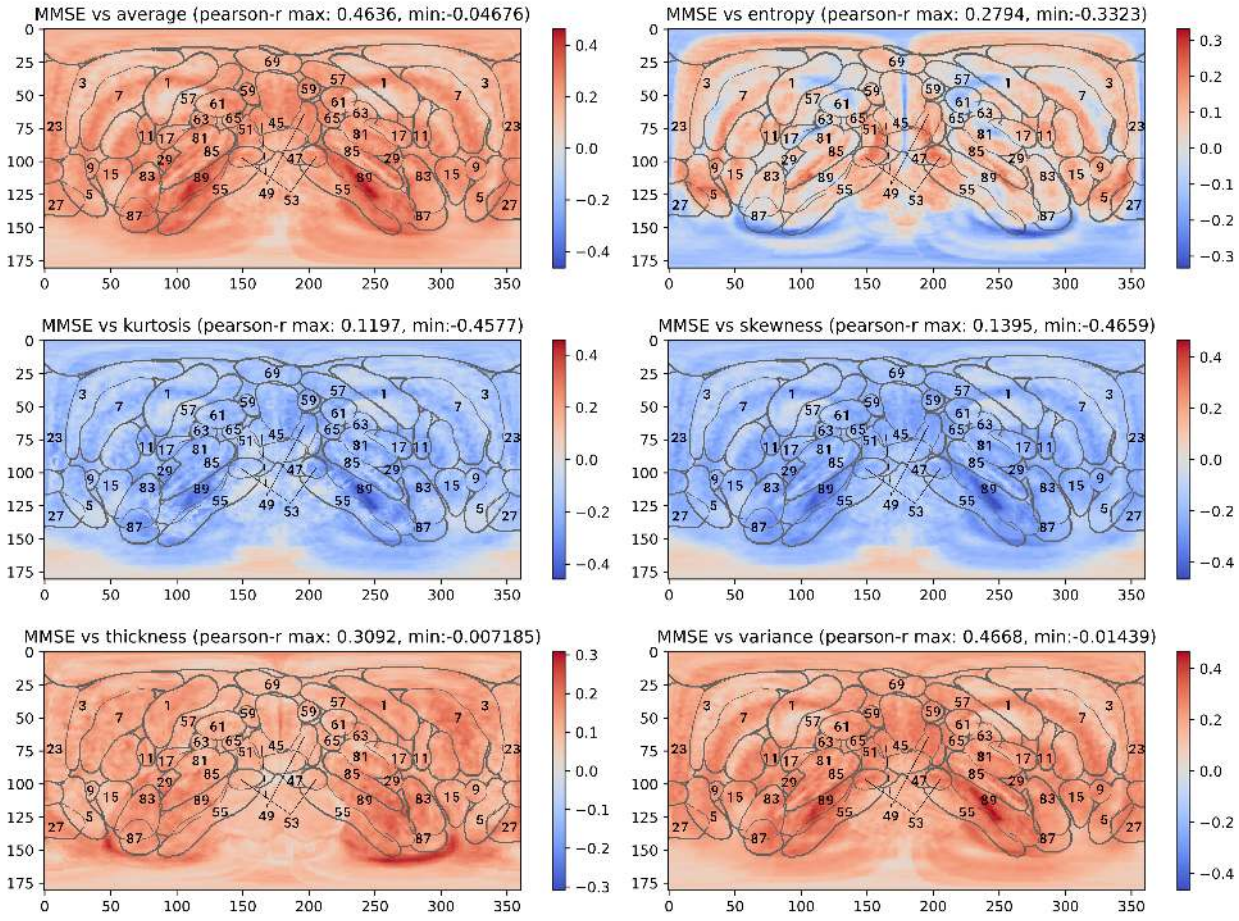

Figure 19: PCC maps computed between the SBM measures for **GM** and the **MMSE**. The reference of **external** structures is superimposed to the figures

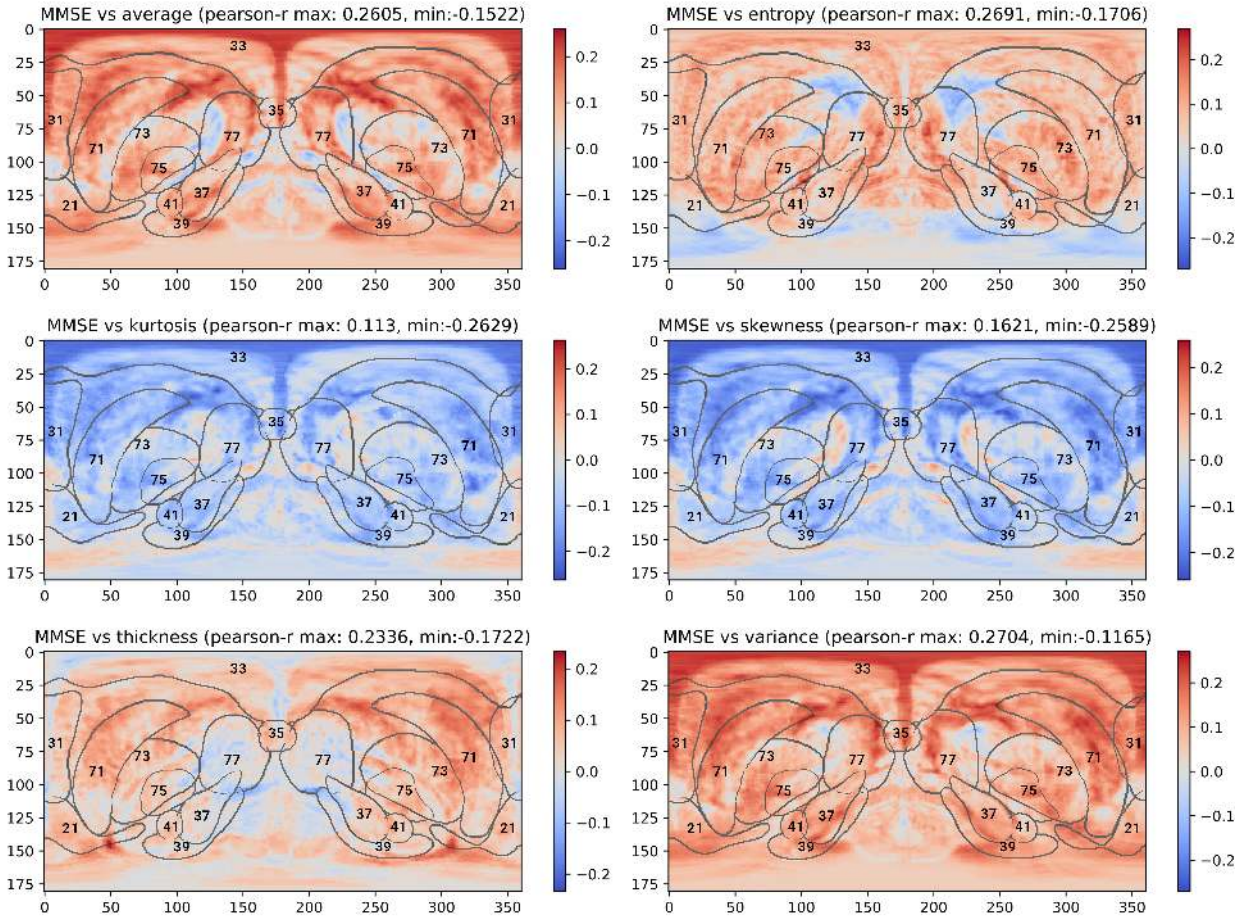

Figure 20: PCC maps computed between the SBM measures for **WM** and the **MMSE**. The reference of **internal** structures is superimposed to the figures

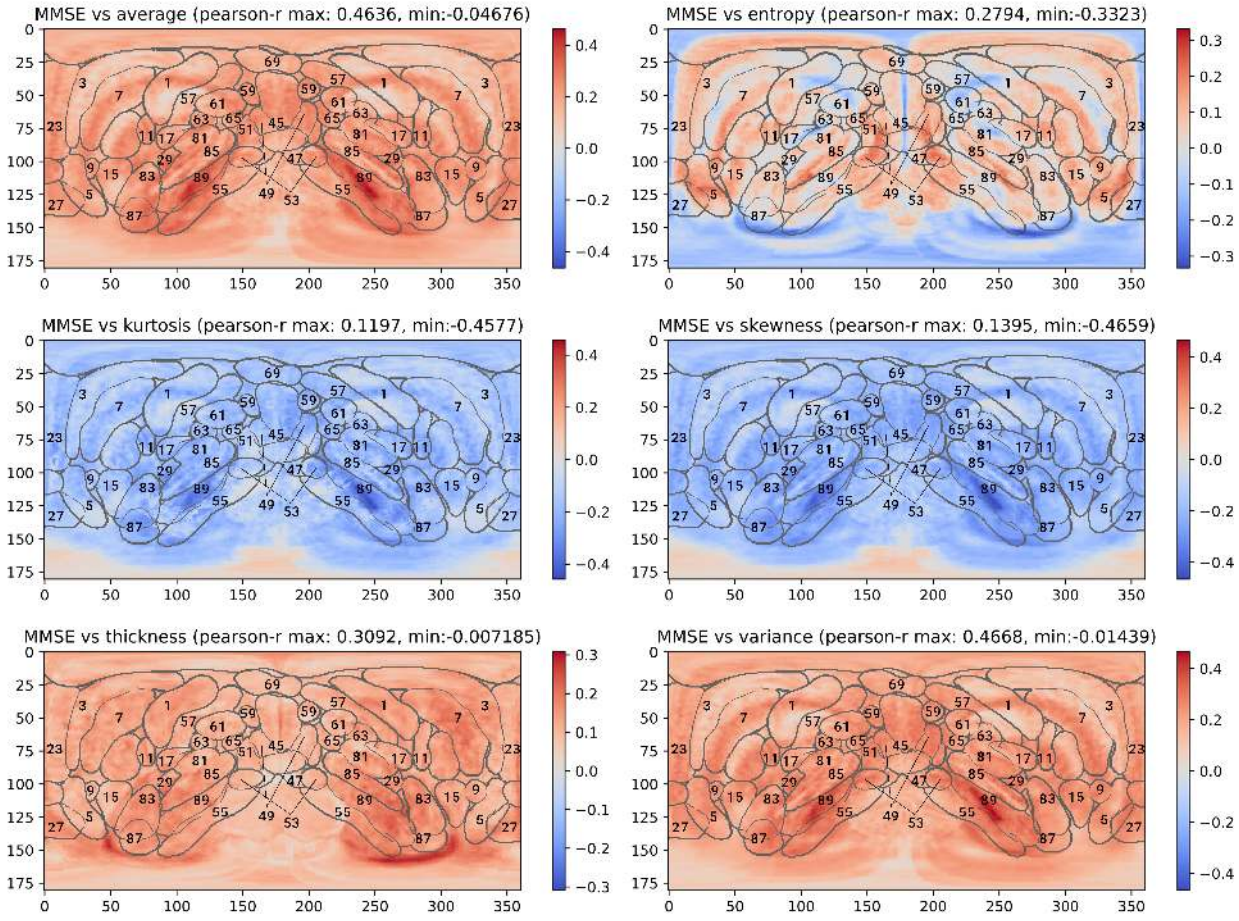

Figure 21: PCC maps computed between the SBM measures for **WM** and the **MMSE**. The reference of **external** structures is superimposed to the figures

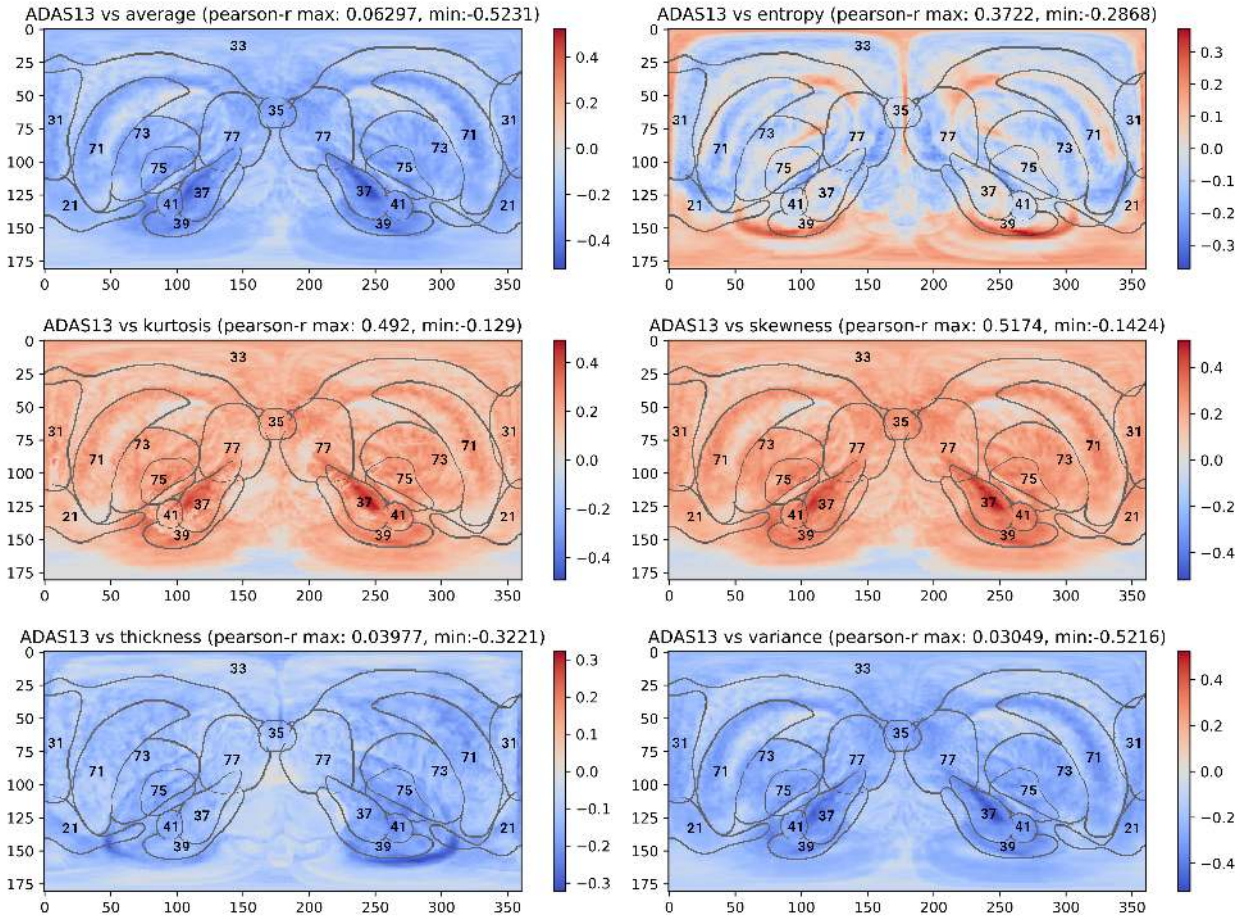

Figure 22: PCC maps computed between the SBM measures for **GM** and the **ADAS13**. The reference of **internal** structures is superimposed to the figures

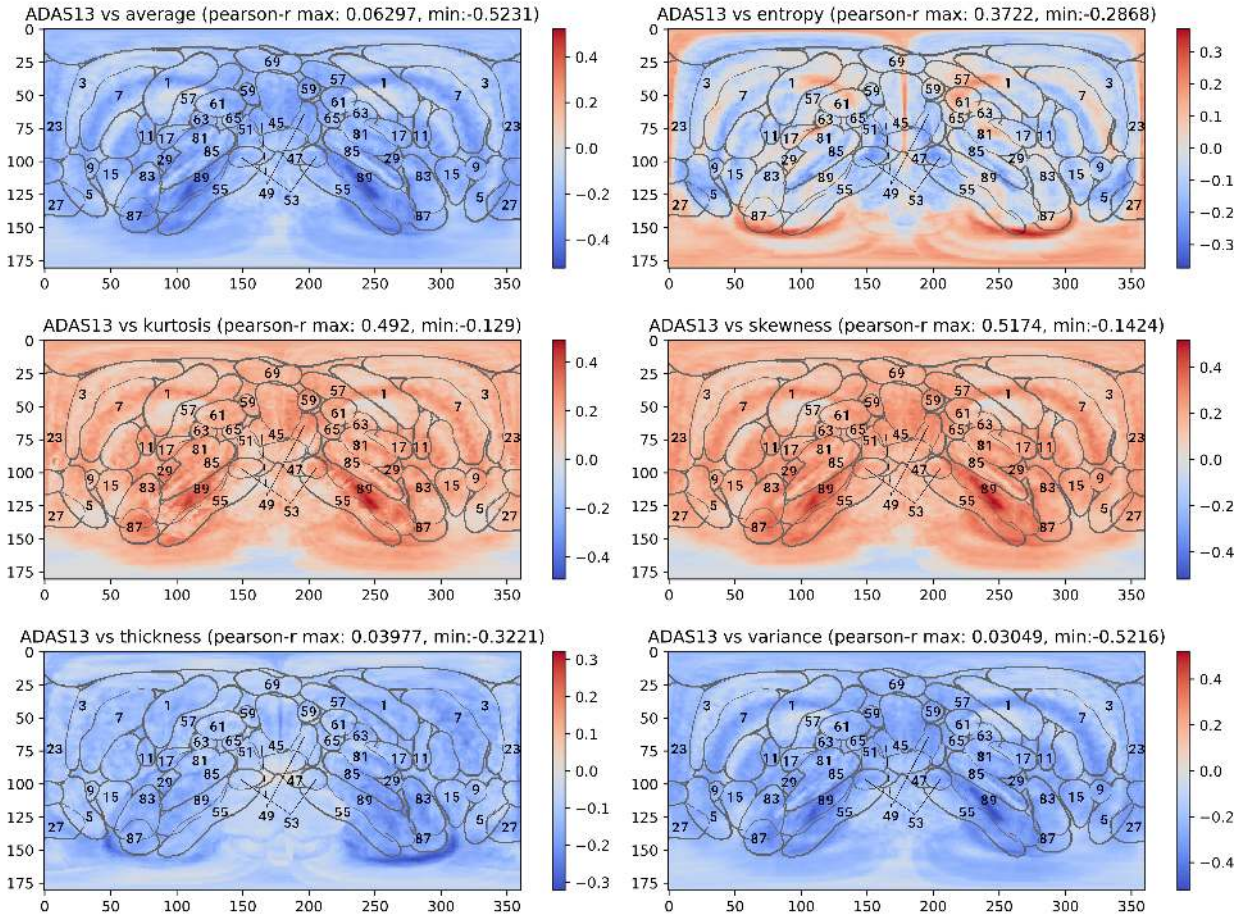

Figure 23: PCC maps computed between the SBM measures for **GM** and the **ADAS13**. The reference of **external** structures is superimposed to the figures

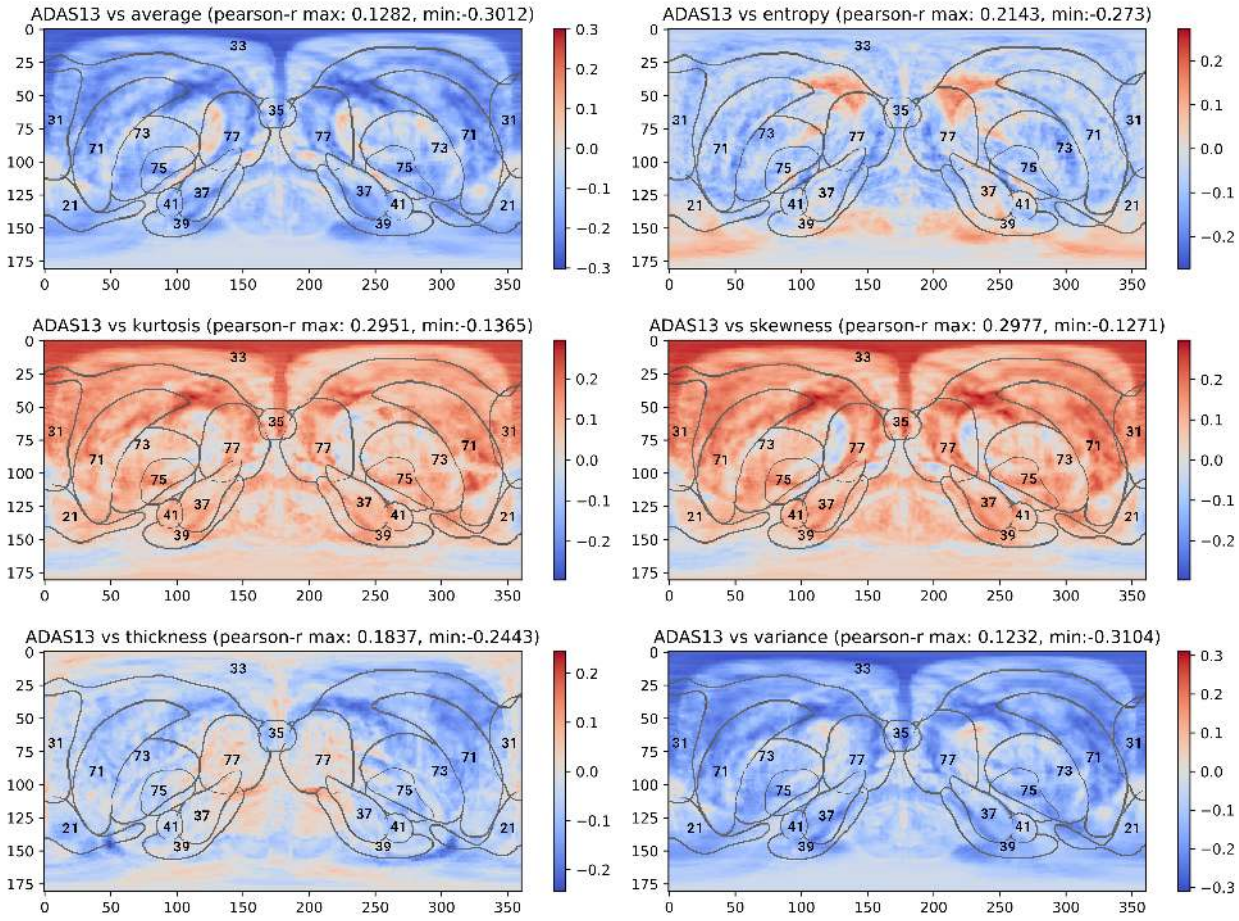

Figure 24: PCC maps computed between the SBM measures for **WM** and the **ADAS13**. The reference of **internal** structures is superimposed to the figures

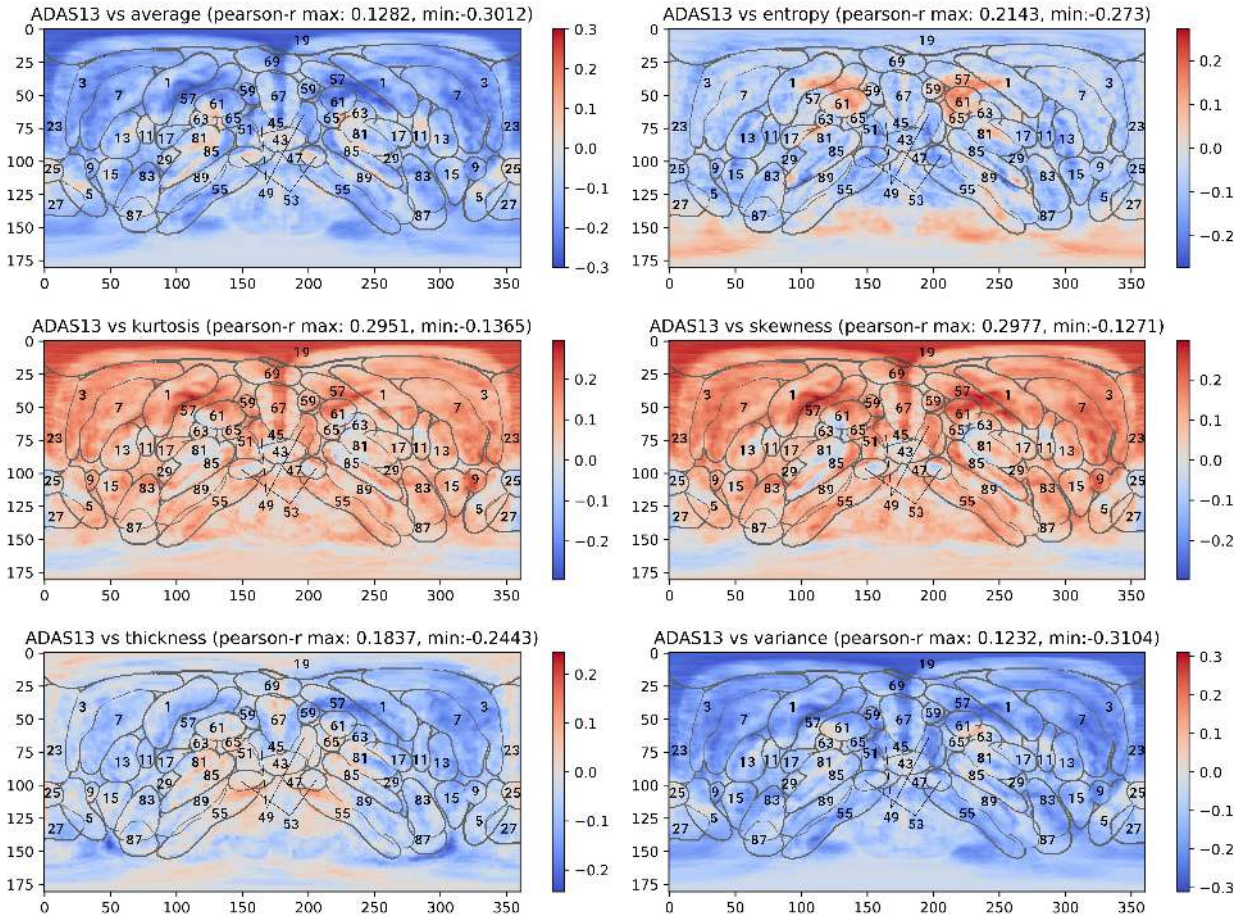

Figure 25: PCC maps computed between the SBM measures for **WM** and the **ADAS13**. The reference of **external** structures is superimposed to the figures